D4.11 - Initial Energy Router

Deliverable ID	**D4.11**
Deliverable Title	**Initial Energy Router**
Work Package	**WP4**
Dissemination Level	**PUBLIC**
Version	**1.0**
Date	**02/11/2018**
Status	**final**
Type	**Prototype**
Lead Editor	**UNINOVA**
Main Contributors	**UNINOVA (Adolfo Steiger Garção, Carlos Roncero-Clemente, João Martins, João Sarraipa, Nuno Vilhena, Vasco Delgado-Gomes)**

Published by the Storage4Grid Consortium

This project has received funding from the European Union's Horizon 2020 research and innovation programme under grant agreement No 731155.

Document History

Version	Date	Author(s)	Description
0.1	2018-06-06	UNINOVA	First draft with sizing and simulation results.
0.2	2018-10-10	UNINOVA	Results of the laboratory tests
0.3	2018-10-29	UNINOVA	Deployment results and figures updated according to the reviewers' requests.
1.0	2018-11-02	UNINOVA	Final version, ready for submission to the EC

Internal Review History

Review Date	Reviewer	Summary of Comments
2018-10-16 (v0.2)	Hamidreza Mirtaheri (ISMB)	Approved: • Once the comment is replied
2018-10-15 (v0.2)	Gustavo Aragón (FRAUNHOFER FIT)	Reviewed: • General minor corrections • Comments on pictures • Missing on-site tests
2018-10-31 (v0.3)	Gustavo Aragón (FRAUNHOFER FIT)	Approved: • General minor corrections
2018-11-01 (v0.3)	Hamidreza Mirtaheri (ISMB)	Approved

Table of Contents

Executive Summary

D4.11 – "Initial Energy Router" presents the sizing, simulation, laboratory tests and on-site tests of the three-phase Energy Router (ER) prototype. The three-phase ER presented in this document was deployed in Skive, Denmark at ENIIG premises. A photovoltaic (PV) system with 245 V Maximum Power Point (MPP) and 1365 W of nominal power is available in the test site. The sizing and simulations in this document were performed taking into consideration theses values.

Different scenarios were defined in order to validate the correct operation of the three-phase ER, namely:

1) PV system is operating at standard conditions, energy storage system (ESS) discharges and DC-AC power converter is injecting pure active power into the main grid.
2) PV system is operating at standard conditions, ESS charges and DC-AC power converter is injecting the remaining pure active power into the main grid.
3) PV system is operating at standard conditions, ESS discharges and DC-AC power converter is injecting reactive power and active power into the main grid.
4) PV system is operating at standard conditions, ESS discharges and DC-AC power converter is injecting unbalanced currents into the main grid.
5) Transient analysis.

A comprehensive simulation study was performed in the PSCAD/EMTDC[i] software to validate the calculated values, the main functionalities, control algorithms, and modulation methods. The five different scenarios were analysed and simulated. The simulations results show a correct operation of the ER in the different scenarios. Furthermore, the different scenarios were also tested in laboratory and at ENIIG's premises, with similar results.

During deployment it was observed that the ER transformer had suffered a mechanical deformation during the transportation to the test site. However, it did not affect its deployment and the tests on the site. Due to this deformation, there is a very small possibility that the transformer creates a hot spot and causes a fire in the room. Since the security of the persons in the building is the top priority, the ER was left disconnected from the grid. The ER correct operation can be verified at any time, with human supervision in the ER room. The ER transformer is planned to be replaced with a new one in the very near future.

In the next prototype document, D4.12 - "Final Energy Router" (M33), it will be presented the single-phase ER prototype that will be deployed in Romania, in the UPB's MicroDERLab facilities.

1 Introduction

D4.11 describes the "Initial Energy Router" prototype, developed by the Storage4Grid project. This prototype describes all the steps made to develop and deploy the three-phase ER prototype. More information regarding the ER controller and the general Storage4Grid architecture, can be retrieved from the related documents summarized in Section 1.2.

1.1 Scope

This prototype deliverable has been developed in Task T4.5 – "Energy Router". Another prototype of this task will be released in M33 as D4.12 – "Final Energy Router", where it will be described the single-phase ER prototype.

1.2 Related documents

ID	Title	Reference	Version	Date
D3.2	Updated S4G Components, Interfaces and Architecture Specification	[S4G-D3.2]	1.0	2018-08-31
D4.9	Updated USM Extensions for Storage Systems	[S4G-D4.9]	1.0	2018-08-31

2 Three-phase Energy Router Prototype Overview

The main blocks diagram of the proposed system is shown in Figure 1. Such system allows the control of several power flow situations. It is composed of the following power stages and sub-systems:

1) PV generation system.
2) DC-DC boost converter as interface between the PV array and the common DC-link.
3) Bidirectional DC-DC buck-boost converter for ESS charging/discharging.
4) Three-phase four-wire DC-AC converter.
5) Utility three-phase grid.

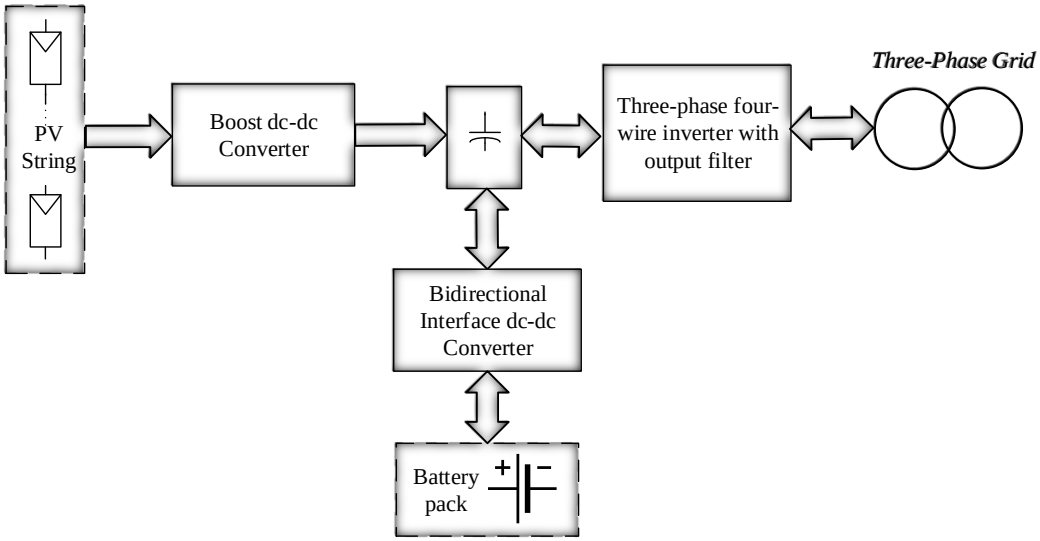

Figure 1. Structure of the power energy conversion system.

The selected topologies of power circuits are depicted in Figure 2.

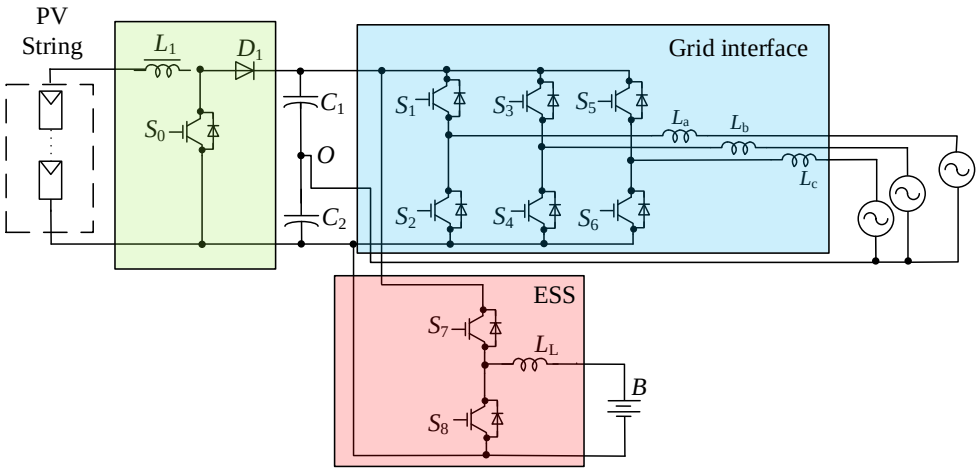

Figure 2. Power topology for the considered energy conversion system.

For the PV interface it was selected a conventional DC-DC boost converter, composed of a pure inductance filter (L_1), a single switch (S_0) and a diode (D_1). The PV panels are directly connected to the DC-DC boost converter, while C_1 and C_2 form the common DC-link for the full system. Its main functionality will be the

maximum power extraction from the PV array (MPPT operation) or to provide any feasible reference value of power (RPPT operation). (Figure 2, subsystem highlighted in green).

Due to the difference in the battery voltage level (96 V) and the considered main DC-link voltage (500 V), a single two-level branch was used in this case to build up the power converter for demanding or injecting power from/to the ESS, working as buck or boost DC-DC converter. It is composed of two switches (S_7 and S_8), and one inductance (L_L). (Figure 2, subsystem highlighted in red).

A three-branches two-level DC-AC power converter with the DC middle point connected to the grid neutral point is in charge of interfacing the energy generation system with the utility three-phase grid. Composed of 6 switches (S_1, …, S_6) and pure inductance filters (L_a, L_b and L_c), this DC-AC converter will be responsible for the main functionalities and services concerning active and reactive power injection, unbalance compensation and grid synchronization. (Figure 2, subsystem highlighted in blue).

3 Sizing of Power Stage for PV interface (DC-DC boost converter)

The following four parameters need to be calculated to size the power circuit that composes the DC-DC boost PV converter:

1) PV input voltage range: minimum PV input voltage ($V_{pv,m}$) and maximum PV input voltage ($V_{pv,M}$).
2) Nominal DC-link voltage (V_{dc_link}).
3) Maximum PV output current ($I_{pv,M}$).
4) Integrated circuit, discrete semiconductor or power module to build the boost converter.

For the Danish residential pilot site, it was considered as input voltage 245 V at the Maximum Power Point (MPP), and as nominal power for the PV array 1365 W at standard conditions of irradiance and temperature. V_{dc_link} is 500 V. It is important to note that this value is feasible due to a 1:2 low frequency transformer. This transformer is installed between the inverter and grid and it is also used to provide galvanic isolation. For safety reasons and possible environmental conditions, it is assumed that $V_{pv,m}$ can get 230 V in case of low irradiance and $V_{pv,M}$ around 310 V (considering this value as open circuit voltage, (V_{oc}) of the PV array).

3.1 Establishment of the maximum switch current and inductor selection

The first step to calculate the switch current is to determine the duty cycle (D_{pv}) for the minimum voltage. This minimum input voltage leads to the maximum switch current. In equation (1), η represents the efficiency of the converter, estimated at 80%. This efficiency is added to the duty cycle calculation since the converter has also to deliver the dissipated energy. This calculation gives a more realistic duty cycle.

$$D_{pv} = 1 - \frac{V_{pv,m} x \eta}{V_{dc\_link}} \quad (1)$$

The next step to calculate the maximum switch current is to determine the inductor ripple current (ΔI_L). The inductor was selected according to equation (2), where f_s is the minimum switching frequency of the converter.

$$L \geq \frac{V_{pv,m} x (V_{dc\_link} - V_{pv,m})}{\Delta I_L x f_s x V_{dc\_link}} \quad (2)$$

The inductor ripple current (ΔI_L) can be estimated using equation (3).

$$\Delta I_L \approx (0.2 \text{to} 0.4) x I_{pv,M} x \frac{V_{dc\_link}}{V_{pv,m}} \quad (3)$$

With equations (1), (2) and (3) it is possible to estimate some of the required values for this sizing stage. Table 1 presents the specifications and rated values and the calculated values.

Table 1. Specifications of DC-DC PV boost converter and calculated values (in bold) for *L*.

Parameter	Value
Maximum power point voltage (V_{mpp})	245 V
Minimum PV input voltage ($V_{pv,m}$)	230 V
Maximum PV input voltage ($V_{pv,M}$)	310 V
Nominal DC-link voltage (V_{dc_link})	500 V
Maximum power point (MPP)	1365 W
Maximum PV output current ($I_{pv,M}$)	4 A
Estimated efficiency of the converter (η)	80 %
Minimum switching frequency (f_s)	15 kHz
Inductor ripple current (Δ_{IL})	**≈1.5 A**
Assumed inductor ripple current (Δ_{IL})	**30 %**
Minimum inductance (L)	**3.3 mH**
Maximum PV duty cycle (D_{pv})	**0.48**

3.2 DC-link capacitor selection

Equation (4) was used to adjust the minimum output capacitor value ($C_{dc\_link,m}$) for a desired output voltage ripple (ΔV_{dc_link}).

$$C_{dc\_link,m} = \frac{I_{pv,M} x D_{pv}}{f_s x \Delta V_{dc\_link}} \quad (4)$$

At the same time, the minimum output voltage ripple is given by equation (5), where ESR is the equivalent series resistance of the used output capacitor. The estimation of this passive component is summarized in Table 2.

$$\Delta Vout = ESR x \left(\frac{I_{pv,M}}{1 - D_{pv}} + \frac{\Delta I_L}{2} \right) \quad (5)$$

Table 2. Specifications of DC-DC PV boost converter and calculated values (in bold) for C.

Parameter	Value
Equivalent series resistance (ESR)	0.25 Ω
Estimated DC-link voltage ripple (ΔV_{dc_link})	**1.69 V**
Considered DC-link voltage ripple (ΔV_{dc_link})	**5 V**
Minimum DC-link capacitor value ($C_{dc\_link,m}$)	**25.6 µF**

4 Sizing of Power Stage for battery interface (DC-DC buck-boost converter)

Similar considerations and procedure were used for sizing the components of the power converter, which will act as power interface with the ESS. The same four values are needed for calculations.

1) Battery pack input voltage range: minimum battery pack input voltage ($V_{bat,m}$) and maximum battery pack input voltage ($V_{bat,M}$).
2) Nominal DC-link voltage (V_{dc_link}).
3) Maximum battery pack output current ($I_{bat,M}$).
4) Integrated circuit, discrete semiconductor or power module to build the boost converter.

For the Danish residential pilot site, it was considered as input voltage 96 V, obtained as serial association of 8x12 V batteries, and as nominal power around 250 W. This ESS voltage level is suitable to interact with the DC-link voltage at 500 V.

4.1 Establishment of the maximum switch current and inductor selection

The first step for calculating the switching current is to determine the duty cycle (D_{bat}) for the minimum voltage. This minimum input voltage leads to the maximum switch current. In equation (6), η represents the efficiency of the converter, estimated at 80% as well.

$$D_{bat} = 1 - \frac{V_{bat,m} x \eta}{V_{dc\_link}} \tag{6}$$

The next step to calculate the maximum switch current is to determine the inductor ripple current (ΔI_L) through the battery. This inductor is calculated using equation (7), where f_s is the minimum switching frequency of the converter.

$$L \geq \frac{V_{bat,m} x (V_{dc\_link} - V_{bat,m})}{\Delta I_L x f_s x V_{dc\_link}} \tag{7}$$

The inductor ripple current (ΔI_L) can be estimated as shown in equation (8).

$$\Delta I_L \approx (0.2\text{to}0.4) x I_{bat,M} x \frac{V_{dc\_link}}{V_{bat,m}} \tag{8}$$

Using equations (6), (7) and (8) it is possible to estimate some of the required values for the inductor sizing. Table 3 presents the specifications and rated values and the calculated values.

Table 3. Specifications of DC-DC buck-boost battery converter and calculated values (in bold) for L.

Parameter	Value
Nominal battery pack voltage (V_{bat})	96 V
Nominal DC-link voltage (V_{dc_link})	500 V
Nominal battery pack power (P_{bat})	250 W
Maximum battery pack output current ($I_{bat,M}$)	2.5 A
Estimated efficiency of the converter (η)	80 %
Minimum switching frequency (f_s)	15 kHz
Inductor ripple current (Δ_{IL})	≈0.2 A
Assumed inductor ripple current (Δ_{IL})	**8 %**
Minimum inductance (L)	**1.5 mH**
Maximum battery duty cycle (D_{bat})	**0.78**

Using the equation (8) to estimate the inductor ripple results in high value due to the difference voltage level between the DC-link (500 V) and the battery side (96 V). The ripple was limited to a value of 0.5 A, to extend the battery useful life

4.2 DC-link capacitor selection

Equation (9) was used to adjust the minimum DC-link capacitor value ($C_{dc\_link,m}$) for a desired DC-link voltage ripple (ΔV_{dc_link}).

$$C_{dc\_link,m} = \frac{I_{bat,M} x D_{bat}}{f_s x \Delta V_{dc\_link}} \quad (9)$$

At the same time, the minimum output voltage ripple is given by equation (10), where ESR is the equivalent series resistance of the used output capacitor. The estimation of this passive component is summarized in Table 4.

$$\Delta V dc\_link = ESR x \left(\frac{I_{bat,M}}{1 - D_{bat}} + \frac{\Delta I_L}{2}\right) \quad (10)$$

Table 4. Specifications of DC-DC buck-boost battery converter and calculated values (in bold) for C.

Parameter	Value
Equivalent series resistance (ESR)	0.25 Ω
Estimated DC-link voltage ripple (ΔV_{dc_link})	**23.1 V**
Considered DC-link voltage ripple (ΔV_{dc_link})	**10 V**
Minimum DC-link capacitor value ($C_{dc\_link,m}$)	**0.1 mF**

5 Sizing of Power Stage for grid interface DC-AC inverter

The component that is necessary to calculate and estimate in a three-phase four-wire DC-AC converter is the output filter. This component is essential for pulse width modulation (PWM) converters. Numerous technical documents cover the output filter design. L, LC, LCL and LLCL output filters are commonly used in this kind of power converter. However, it was selected a pure L filter to avoid resonance frequencies.

There are several criteria that can be considered for L-filter selection. For instance, the ripple criteria ensures that the error between the reference current and the grid injected current by the converter is within a margin regulated by the power quality standards (usually between 5% and 15%). Another criterion is based on the current ripple calculation on the switching harmonic. Figure 3 shows a typical harmonic spectrum of the DC-AC inverter. It is possible to define the converter voltage harmonic at the switching frequency.

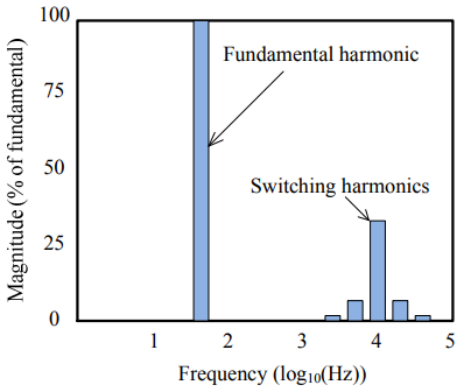

Figure 3. Typical harmonic spectrum of the grid current.

Assuming that the current ripple is directly and exclusively influenced by the switching frequency, equation (11) is considered, where I_{SW} is the grid RMS harmonic current at the switching frequency, I_1 is the RMS value of the current fundamental harmonic of the grid.

$$THD_I \approx \sqrt{\frac{I_{SW}^2}{I_1^2}} = \frac{I_{SW}}{I_1} \tag{11}$$

The current ripple through the converter side to the grid side can be computed upon consideration that at high frequencies, the converter is a harmonic generator, while the grid can be considered as a short circuit, as shown in Figure 4. This is expressed in equation (12), where h_{SW} – the number of switching harmonic, ω_1 – fundamental harmonic, and total filter inductance $L_f=L_i+L_{g2}$.

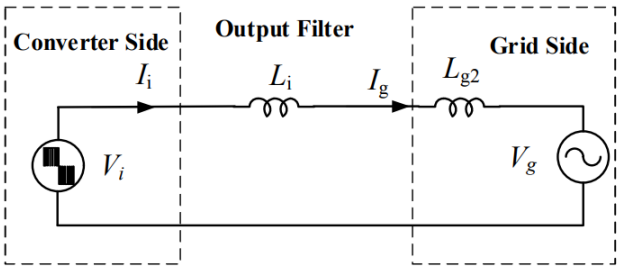

Figure 4. Equivalent grid-connected converter with L filter.

$$G_L(h_{sw}) = \frac{I_g(h_{sw})}{V_i(h_{sw})} = \left| \frac{-j}{\omega_1 h_{sw}(L_i + L_{g2})} \right| \quad (12)$$

From equation (12), the current ripple is defined as show in equation (13).

$$I_{SW} = I_g(h_{sw}) = V_i(h_{sw}) \frac{1}{\omega_1 h_{sw} L_f} \quad (13)$$

To estimate the inductance value, it was necessary to establish the harmonic component of the converter output voltage at the switching frequency V_i(hSW). Considering unity power factor and equations (11) and (13), equation (14) can be written, where P is the rated power.

$$L_f \geq \frac{V_i(h_{sw}) V_g}{\omega_1 h_{sw} P THD_I} \quad (14)$$

As the voltage harmonic component at the switching frequency is unknown, the current ripple can be estimated directly from this calculation using the inverter voltage waveform. Typically, such approach gives the same result, since there is a proportional relation between the two magnitudes: ripple and content of harmonics. Table 5 presents the specification, rated values and the calculated values.

Table 5. Specifications of three-phase four-wire DC-AC converter and calculated values (in bold) for L

Parameter	Value
Rated Power of Inverter (P)	5000 W
RMS Grid phase to neutral voltage (V_g)	230 V
Converter voltage at switching frequency ($V_i(h_{sw})$)	23 V (10%)
h_{sw}	300 (15 kHz)
Fundamental frequency (ω_1)	50 Hz
THD_I	5 %
Minimum inductance filter (L)	**1.5 mH**

6 Control algorithms

The general block diagram of the initially proposed control structure is shown in Figure 5. The DC-AC converter operates with a direct (d) component reference current ($i_{d,ref}$) obtained by a DC-link control loop. This control loop forces the system to maintain a constant voltage at the desired level. At the same time, it is able to inject different power between phases. The four-wire system allows to inject asymmetrical phase current to the grid. The current tracking control is based on the predictive control type with a dead-beat current controller.

The power exchange between battery and DC-link is controlled using the external control block according to the battery state of charge (SoC) and user specifications. The DC-DC PV boost converter will extract the maximum power from the PV array or any feasible active power reference.

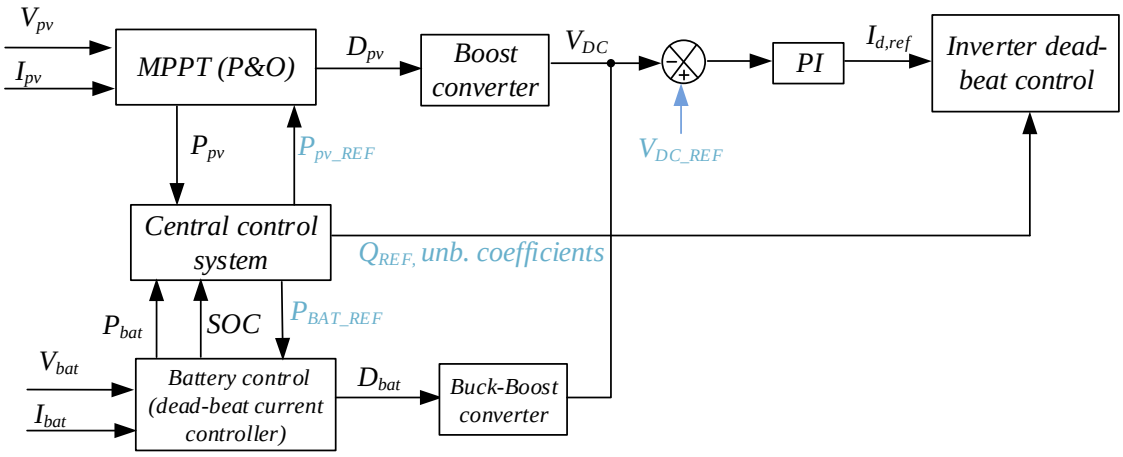

Figure 5. Block diagram of the Initial proposed control strategy.

7 Simulation results

In order to validate the calculated parameters, as well as the main functionalities, control algorithms and modulation methods, a comprehensive simulation study was performed using PSCAD/EMTDC[i] software. All the details and studied scenarios are given in this section. It is important to note that the required measurements are sampled to match with the control frequency rate implemented in the ER controller, making the simulation more realistic for further real implementation. The different scenarios analysed and simulated, were:

1) PV system is operating at standard conditions, ESS discharges and DC-AC power converter is injecting pure active power into the main grid.
2) PV system is operating at standard conditions, ESS charges and DC-AC power converter is injecting the remaining pure active power into the main grid.
3) PV system is operating at standard conditions, ESS discharges and DC-AC power converter is injecting reactive power and active power into the main grid.
4) PV system is operating at standard conditions, ESS discharges and DC-AC power converter is injecting unbalanced currents into the main grid.
5) Transient analysis.

7.1 Scenario 1

The first scenario aims to validate the steady state conditions. Figure 6 shows the evolution of reference MPP current. This magnitude is obtained by using the MPPT algorithm based on Perturb and Observe (P&O) with adaptive step. The PV voltage and current track the nominal values with accuracy in the steady state.

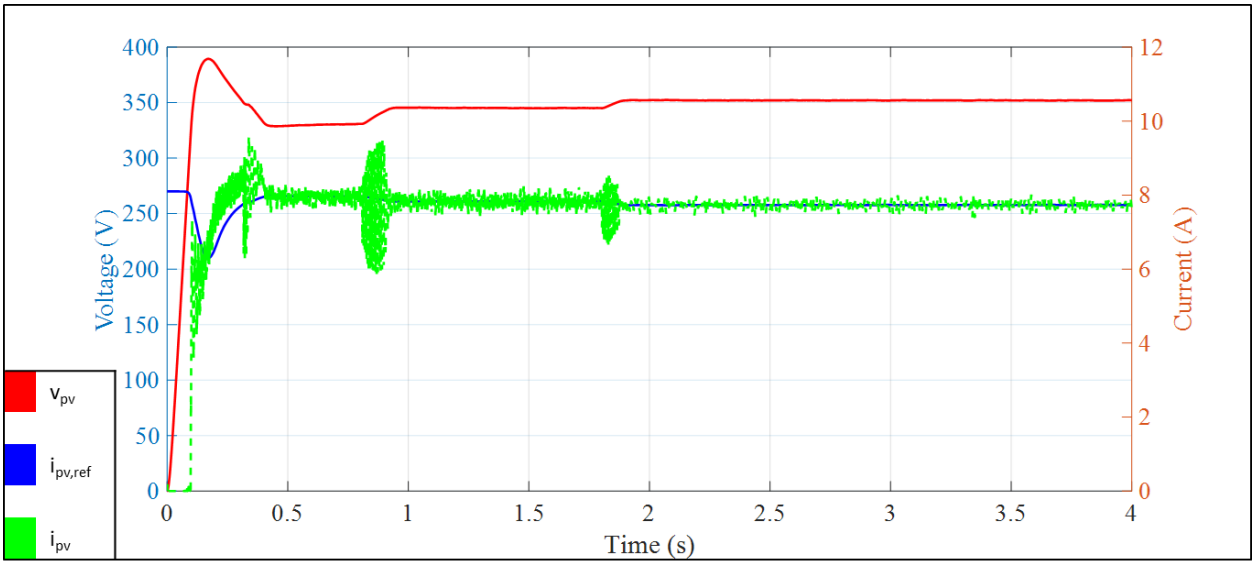

Figure 6. Scenario 1: PV voltage (v_{pv}), reference MPP current ($i_{pv,ref}$) and PV current (i_{pv}).

Figure 7 shows the PV current in steady state, once the MPPT is achieved. The PV current ripple (Figure 8) demonstrates that this value is under the design limits (Table 1).

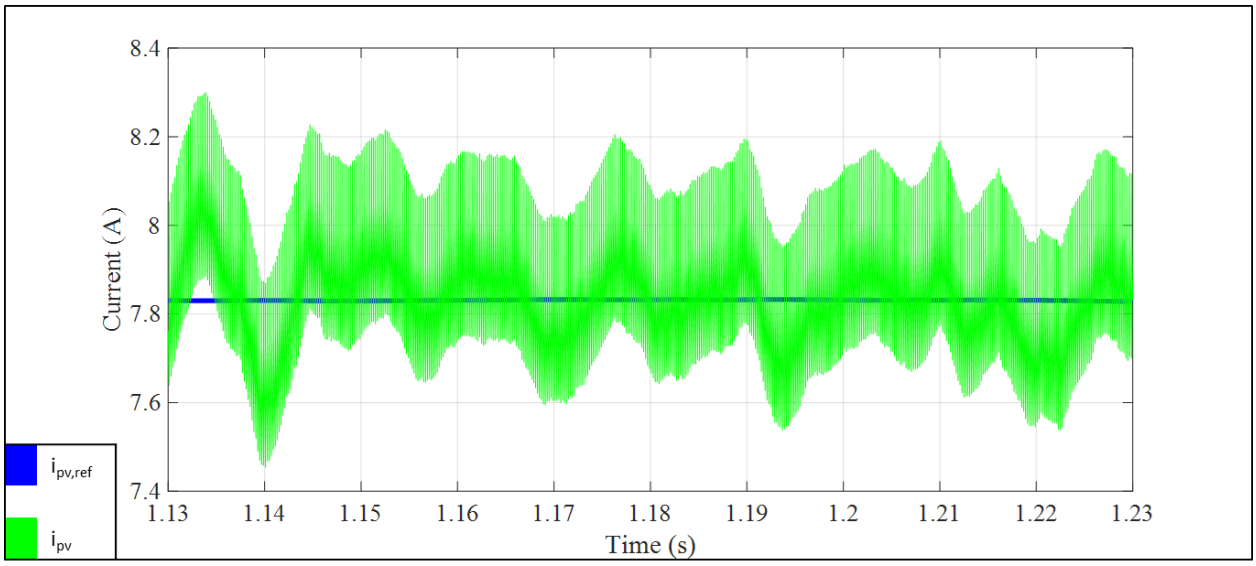

Figure 7. Scenario 1: PV current reference ($i_{pv,ref}$) and the obtained PV current ripple (i_{pv}).

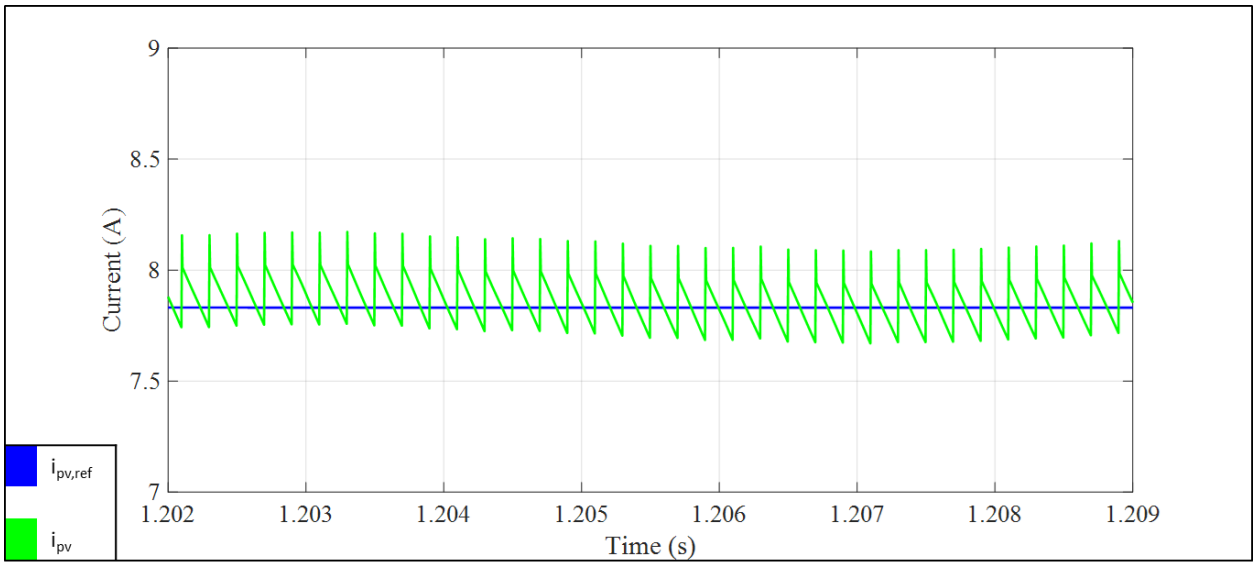

Figure 8. Scenario 1: Detail of the PV current ripple (i_{pv}) according to the PV current reference ($i_{pv,ref}$).

The magnitudes analysis of the DC-DC buck-boost battery converter is shown in Figure 9. The battery is discharged with a reference current of 10 A and the battery SoC decreases. The battery current ripple is again under the sizing specifications (8 %). The PV power and battery powers are injected to the main grid using the DC-AC converter. Sinusoidal currents are obtained and injected to the grid, as shown in Figure 10.

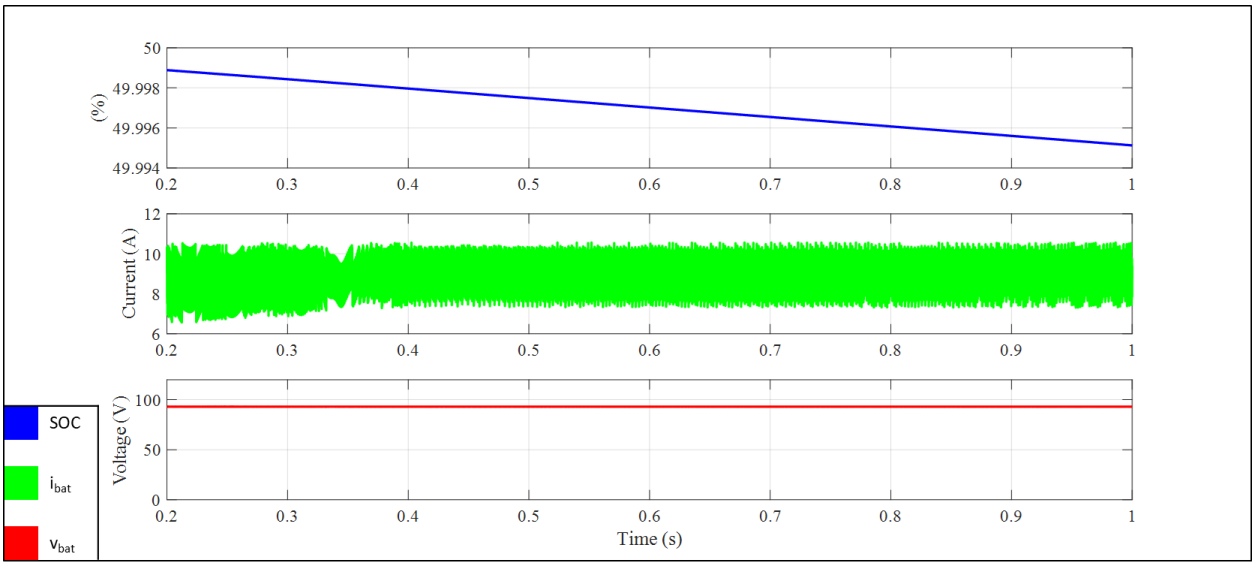

Figure 9. Scenario 1: Main magnitudes of the DC-DC buck-boost battery converter: ESS SoC, battery current (i_{bat}) and battery voltage (v_{bat}).

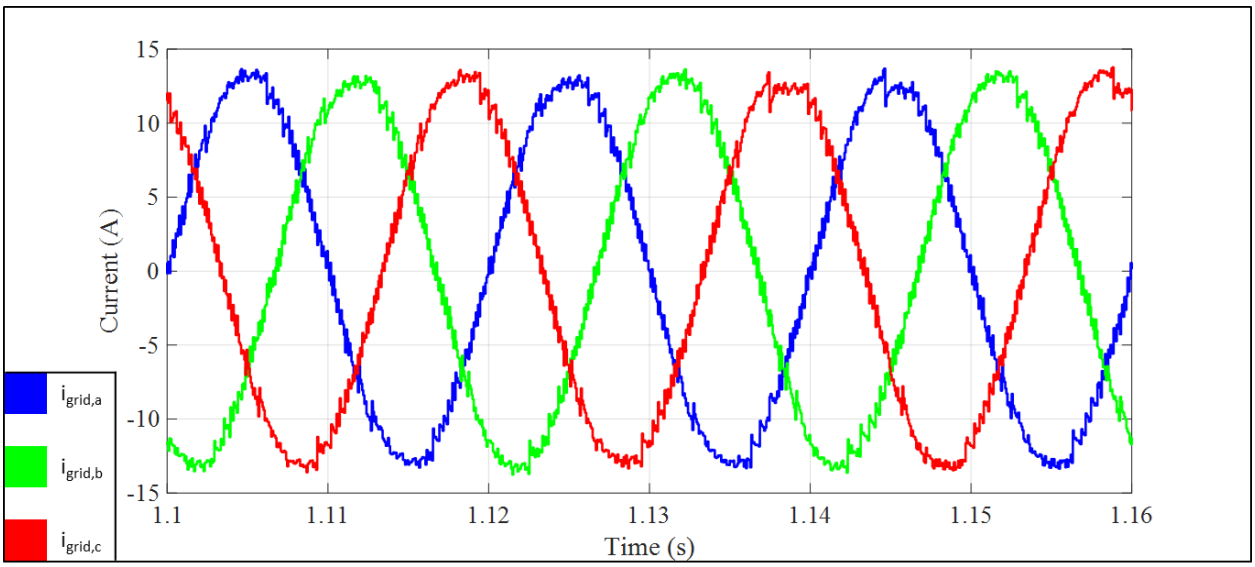

Figure 10. Scenario 1: Output currents ($i_{grid,a}$, $i_{grid,b}$, $i_{grid,c}$) of the DC-AC converter.

7.2 Scenario 2

This scenario considers that ESS must be charged, but the PV power is higher than the reference battery power, so the excess power will be injected to the grid with unitary power factor.

The same response as in scenario 1 is provided by the PV boost converter. Figure 11 depicts the evolution of reference MPP current. This magnitude is obtained by using the MPPT algorithm based on P&O. The PV voltage and current track the nominal values with accuracy in the steady state.

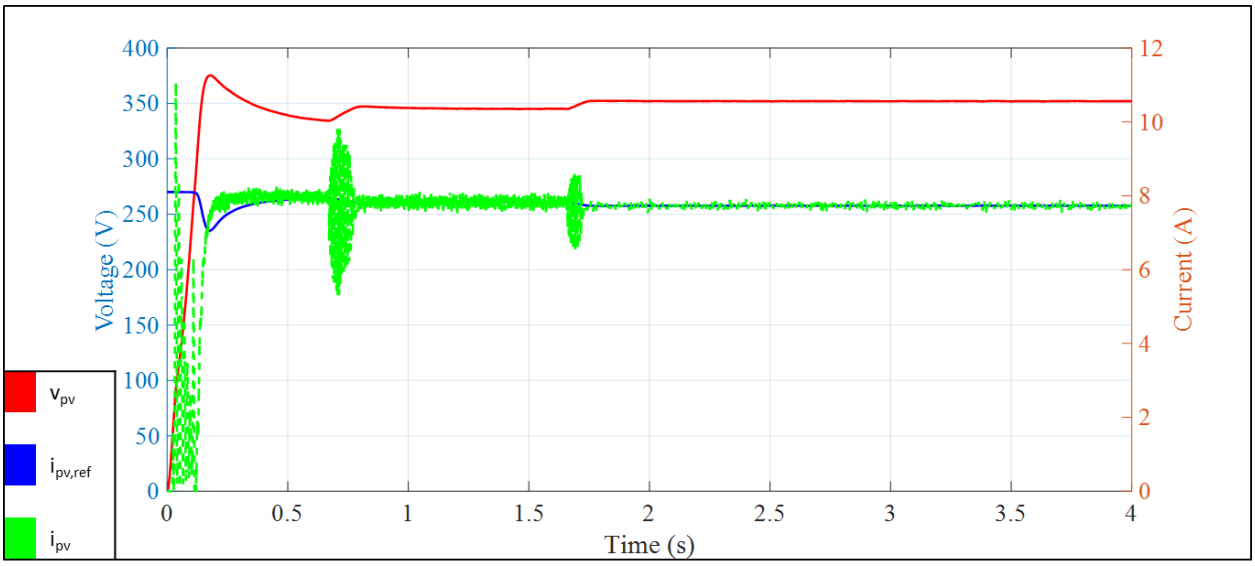

Figure 11. Scenario 2: PV voltage (v_{pv}), reference MPP current ($i_{pv,ref}$) and PV current (i_{pv}).

In this scenario, the DC-DC buck-boost battery converter is working as shown in Figure 12. The battery is charged with the PV generation with a reference current of 10 A and the battery SoC increases. The battery current ripple is again under the sizing specifications (8 %). The remaining PV power is injected to the main grid using the DC-AC converter. The output currents are depicted in
Figure 13.
The main DC-link voltage is also represented in Figure 14 and its value is maintained in 500 V as defined by the reference value, which assures the proper operation of the DC-link control loop.

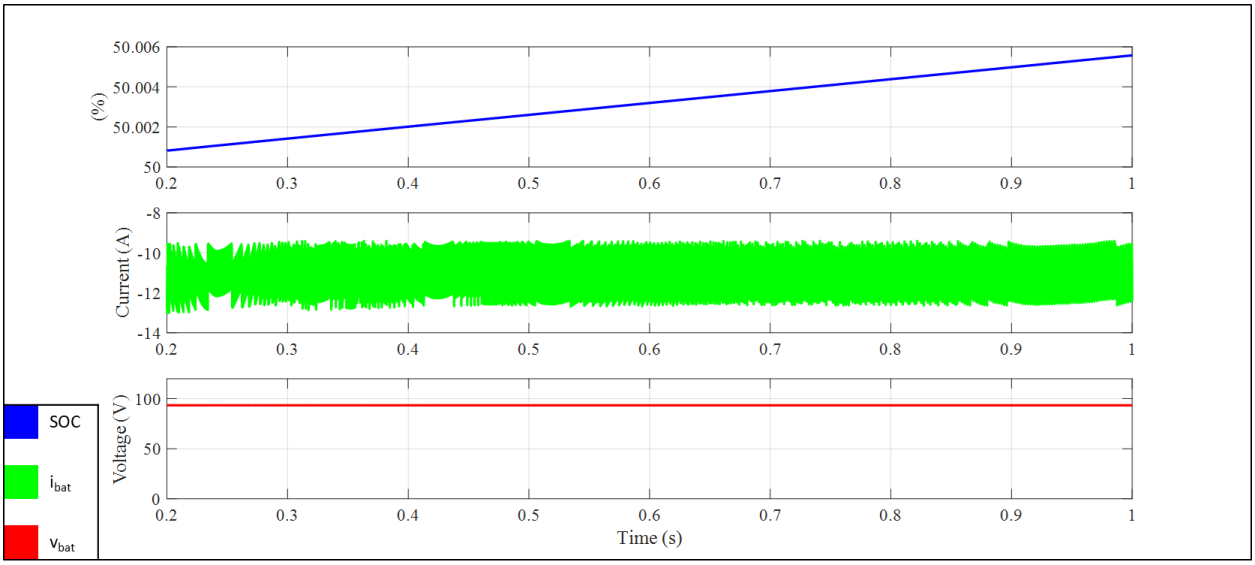

Figure 12. Scenario 2: Main magnitudes of the DC-DC buck-boost battery converter: ESS SoC, battery current (i_{bat}) and battery voltage (v_{bat}).

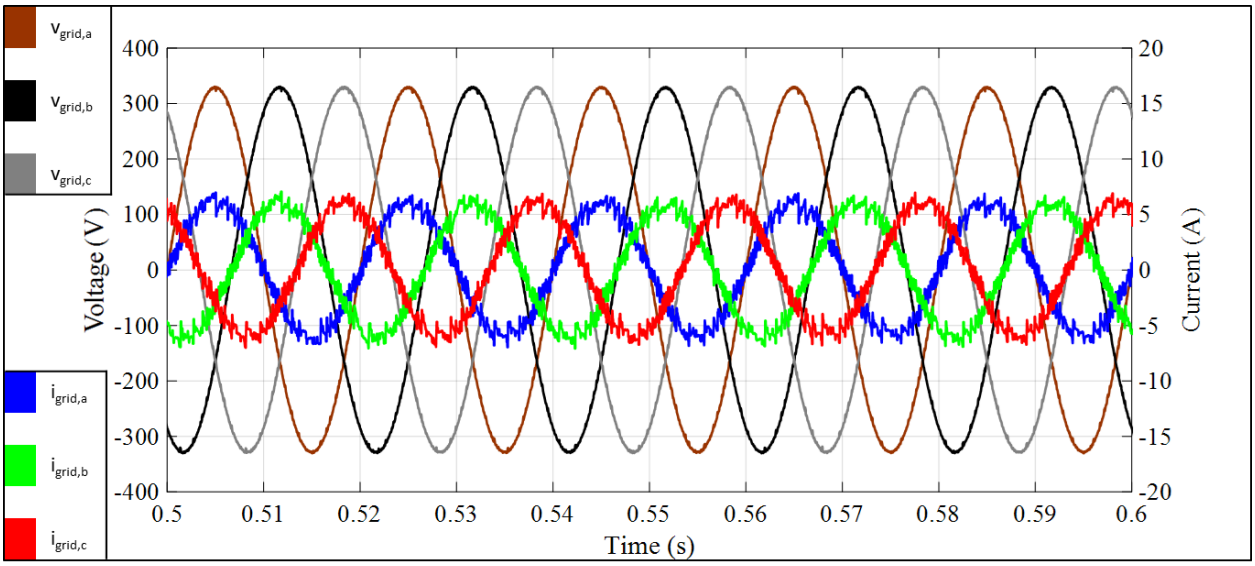

Figure 13. Scenario 2: Output currents ($i_{grid,a}$, $i_{grid,b}$, $i_{grid,c}$) and grid voltages ($v_{grid,a}$, $v_{grid,b}$, $v_{grid,c}$) of the DC-AC converter.

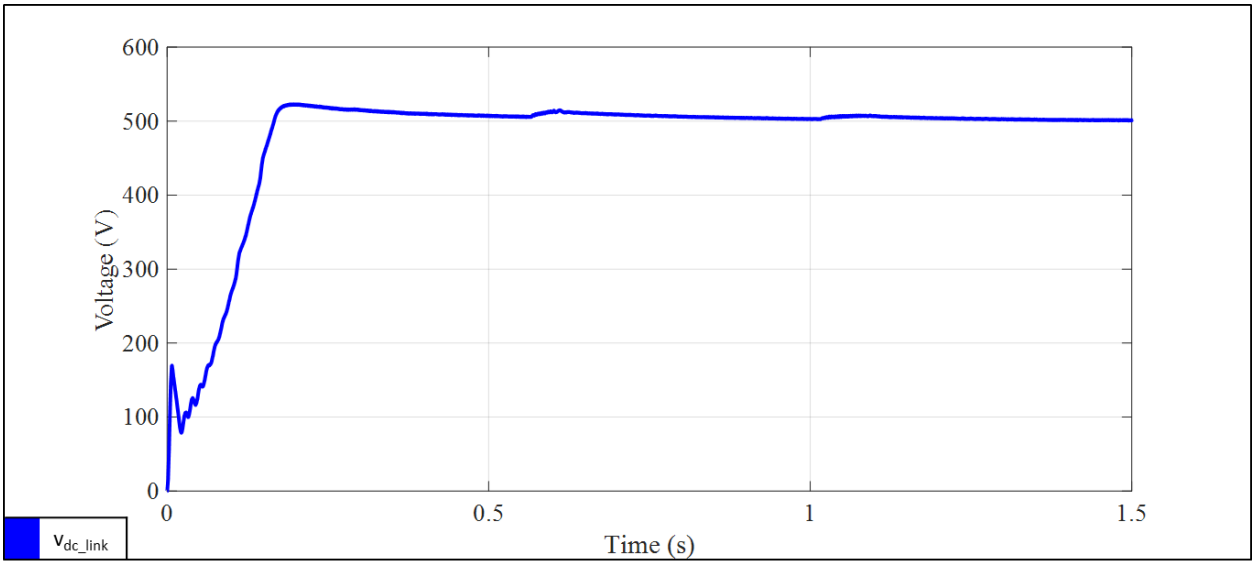

Figure 14. Scenario 2: Evolution of the main DC-link voltage (v_{dc_link}) during start-up.

7.3 Scenario 3

This scenario demonstrates the ability of the DC-AC power converter to inject reactive power. The functionality helps to restore the voltage at the point of common coupling, being mandatory by the main European regulations (e.g. CEI 0-21[ii], FGW TR3[iii], Spanish Decree Law 1565/2010[iv]).

In this scenario, the PV power and battery power are injected to the main grid and a reference reactive power is also given. Figure 15 shows the shift between grid voltages and currents, validating the proper operation of the full system.

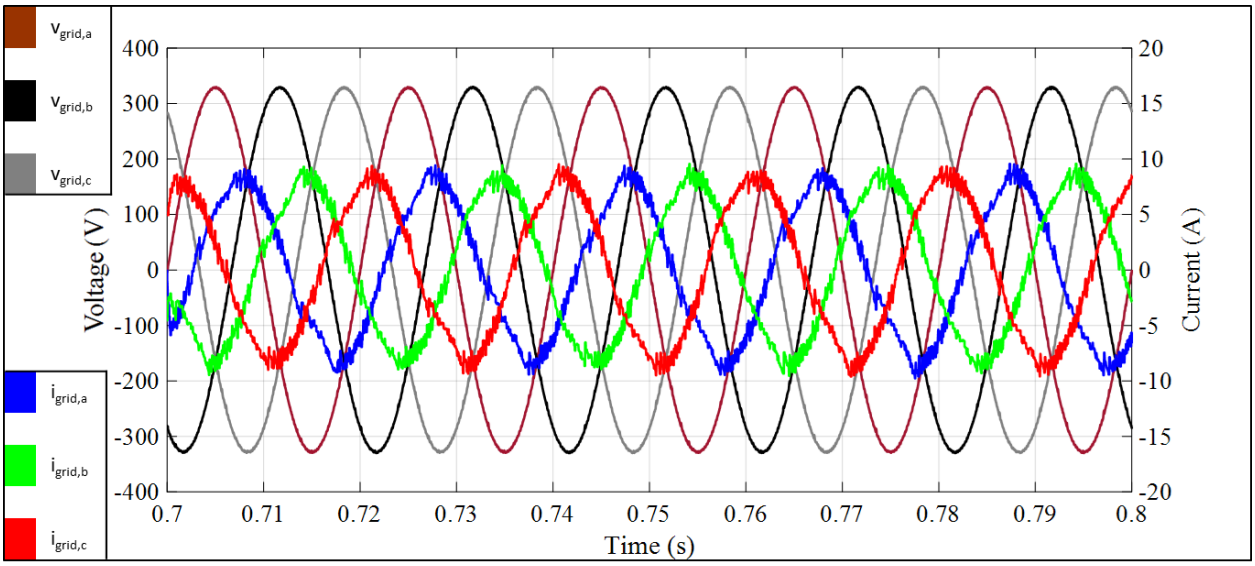

Figure 15. Scenario 3: Output currents ($i_{grid,a}$, $i_{grid,b}$, $i_{grid,c}$) and grid voltages ($v_{grid,a}$, $v_{grid,b}$, $v_{grid,c}$) of the DC-AC converter.

7.4 Scenario 4

This scenario illustrates the functionality required for supplying unbalanced loads or for the compensation effects of unbalance voltages in the grid. Different current references per phases are introduced and a proper tracking is observed (Figure 16). In this scenario, the current flowing through the neutral wire is not zero.

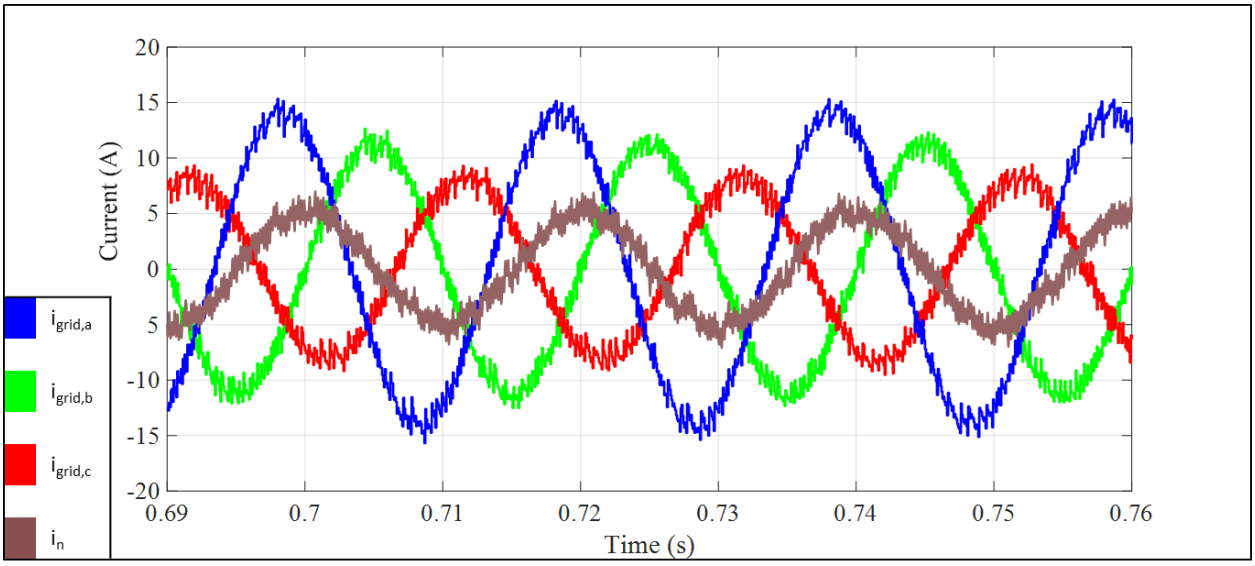

Figure 16. Scenario 4: Output currents ($i_{grid,a}$, $i_{grid,b}$, $i_{grid,c}$) and neutral current (i_n) of the DC-AC converter.

7.5 Scenario 5

In the last scenario, the transient response under active power reference and reactive power reference step values are simulated and observed. This situation is critical to prevent further damage of the real system. PV irradiance may change as well as the main reference given by the ER control system. Different steps in active power can be delivered using the ESS if the battery SoC is within the limits. Figure 17 shows the output currents

injected to the grid and the transient responses of the battery converter (Figure 18). Figure 19 shows the evolution of injected current under a reactive power step reference.

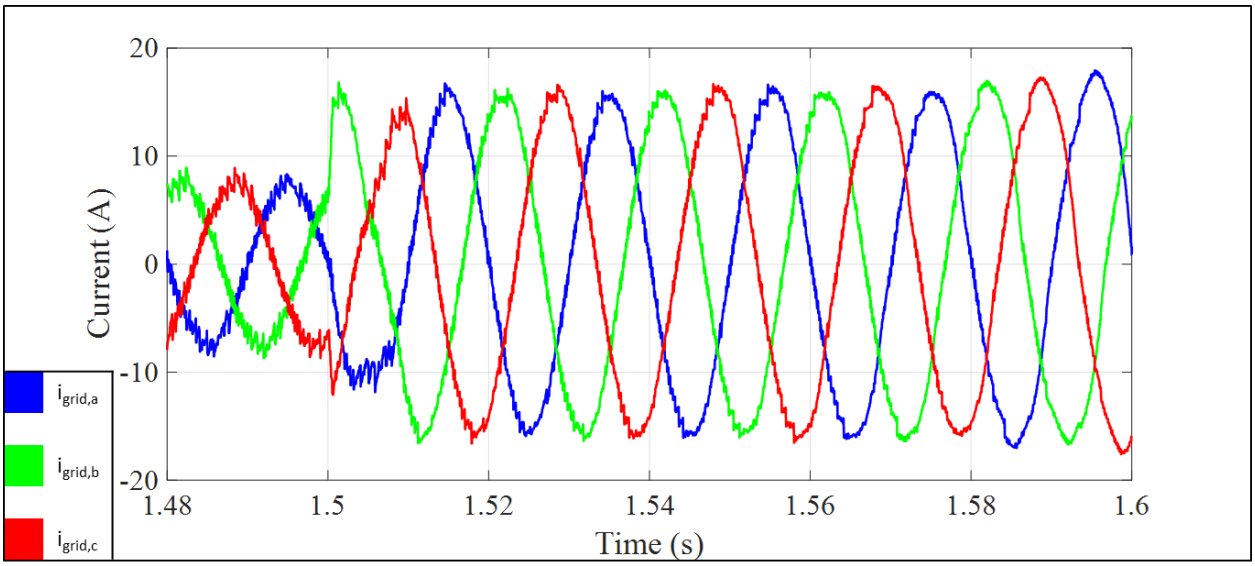

Figure 17. Scenario 5: Evolution of the output currents ($i_{grid,a}$, $i_{grid,b}$, $i_{grid,c}$) of the DC-AC converter under an active power step reference.

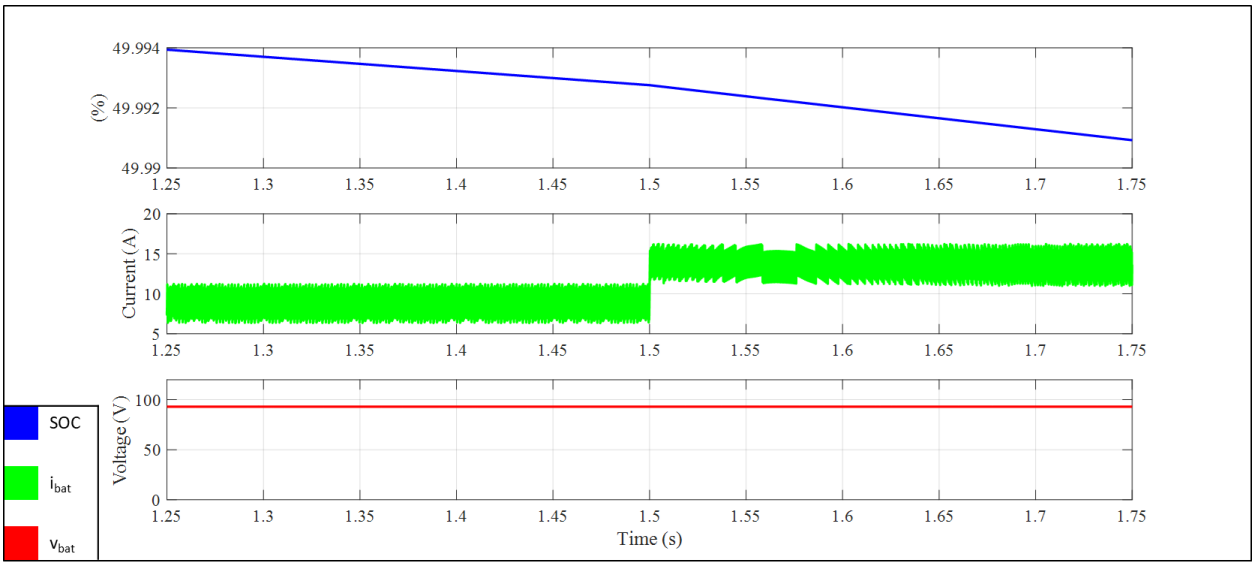

Figure 18. Scenario 5: Main magnitudes of the DC-DC buck-boost battery converter: ESS SoC, battery current (i_{bat}) and battery voltage (v_{bat}).

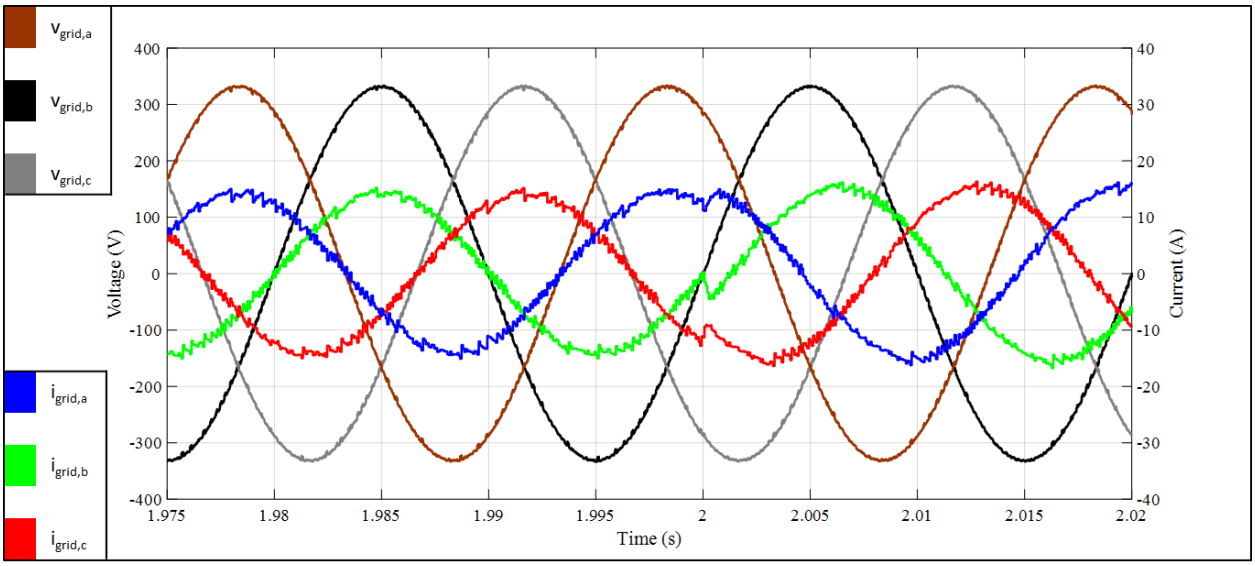

Figure 19. Scenario 5: Evolution of the output currents ($i_{grid,a}$, $i_{grid,b}$, $i_{grid,c}$) and grid voltages ($v_{grid,a}$, $v_{ggrid,b}$, $v_{grid,c}$) under a reactive power step reference.

8 Laboratory tests

The assembled prototype based on the aforementioned specifications and sizing was tested in different scenarios to validate the proper performance. The Insulated-Gate Bipolar Transistors (IGBTs) selected for the power electronic converters were the SEMIKRON SKM50GB12T4 branch module.
The photovoltaic array is emulated by means of the Chroma solar array simulator 62000H-S, using the PV panels specifications available on the test site (PV panel ET M5772185BB). The ESS is composed by a serial connection of 8 lead-acid type batteries. The main parameters of the experimental tests are described in Table 6.

Table 6. Laboratory specifications of the experimental setup.

PV, ESS and grid	Parameter	Value
PV parameters per panel in standard conditions (array is composed by 7 panels in serial)	Open circuit voltage (V_{oc})	45.03 V
	Short-circuit current (I_{sc})	5.47 A
	Voltage at maximum power (V_{mpp})	36.3 V
	Current at maximum power (I_{mpp})	5.11 A
ESS parameters per single battery (pack is composed by 8 batteries connected in serial)	Battery voltage	12 V
	Battery capacity	15 Ah
Utility grid	Grid voltage	230 V

The previous described five scenarios were tested in laboratory, namely:

1) PV system is operating at standard conditions, ESS discharges and DC-AC power converter is injecting pure active power into the main grid.
2) PV system is operating at standard conditions, ESS charges and DC-AC power converter is injecting the remaining pure active power into the main grid.
3) PV system is operating at standard conditions, ESS discharges and DC-AC power converter is injecting reactive power and active power into the main grid.
4) PV system is operating at standard conditions, ESS discharges and DC-AC power converter is injecting unbalanced currents into the main grid.
5) Transient analysis.

8.1 Scenario 1

The first test aims to validate the proper operation of the full system in terms of active power balance between the energy source, storage system and the utility grid. The main waveforms are represented in Figure 20. i_{pv} shows a good tracking of the current at maximum power (i_{mpp}) with its current ripple within the limit. The battery current (i_{bat}) is also depicted when the ESS is discharged with a $P_{bat,ref}$ equal to 100 W. The resulting power is injected into the utility grid. Phase A of the current ($i_{grid,a}$) and phase A of the voltage ($v_{grid,a}$) present the same shift. It is important to note that the grid current distortion is explained by the open-circuit current demanded by the 1:2 isolation transformer connected between the three-phase inverter and the main grid.

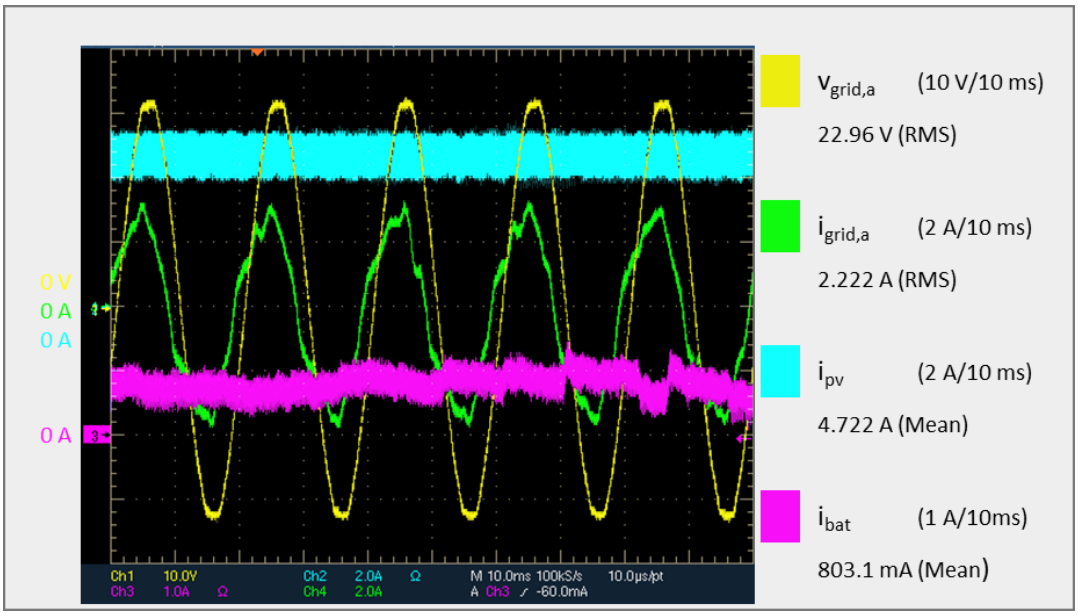

Figure 20. Scenario 1: Injected current to the grid in phase A ($i_{grid,a}$), grid voltage in phase A ($v_{grid,a}$), PV current (i_{pv}) and battery current (i_{bat}).

8.2 Scenario 2

In scenario 2, a similar test as in scenario 1 was carried out, in order to test the bidirectional capability of the buck-boost ESS power converter. In this scenario (Figure 21), i_{pv} shows a good tracking of the current at maximum power (i_{mpp}), but the battery current (i_{bat}) gets a negative value since the ESS is being charged with a $P_{bat,ref}$ equals to -100 W. The remaining power is injected to the utility grid, the phase A of the current ($i_{grid,a}$) and the phase A of the voltage ($v_{grid,a}$).

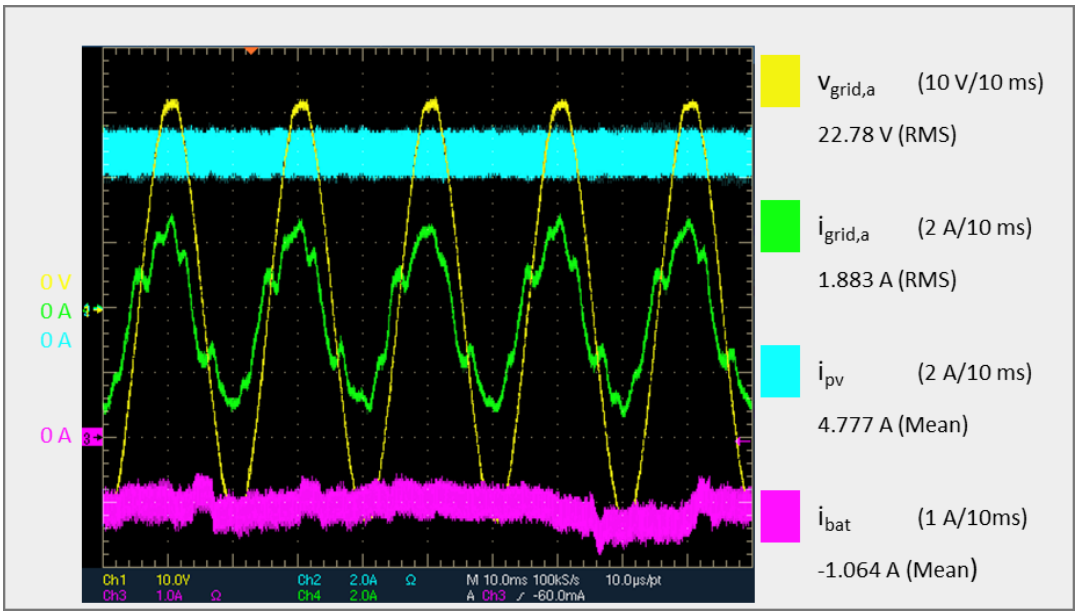

Figure 21. Scenario 2: Injected current to the grid in phase A ($i_{grid,a}$), grid voltage in phase A ($v_{grid,a}$), PV current (i_{pv}) and battery current (i_{bat}).

8.3 Scenario 3

In this scenario, the ER shows how it is able to provide ancillary services to the main grid in cases where the grid voltage needs to be supported. This situation is represented in Figure 22, where i_{pv} shows the PV current which is extracting the maximum power from the PV source. The battery current (i_{bat}) has a discharging value corresponding to 100 W. The resulting active power and reactive power ($Q_{grid,ref}$ equals to 900 VAr) is injected to the utility grid. It can be observed that the grid current ($i_{grid,a}$) and grid voltage ($v_{grid,a}$) are shifted. The RMS value of the grid current is increased due to the quadrature (q) component of the current.

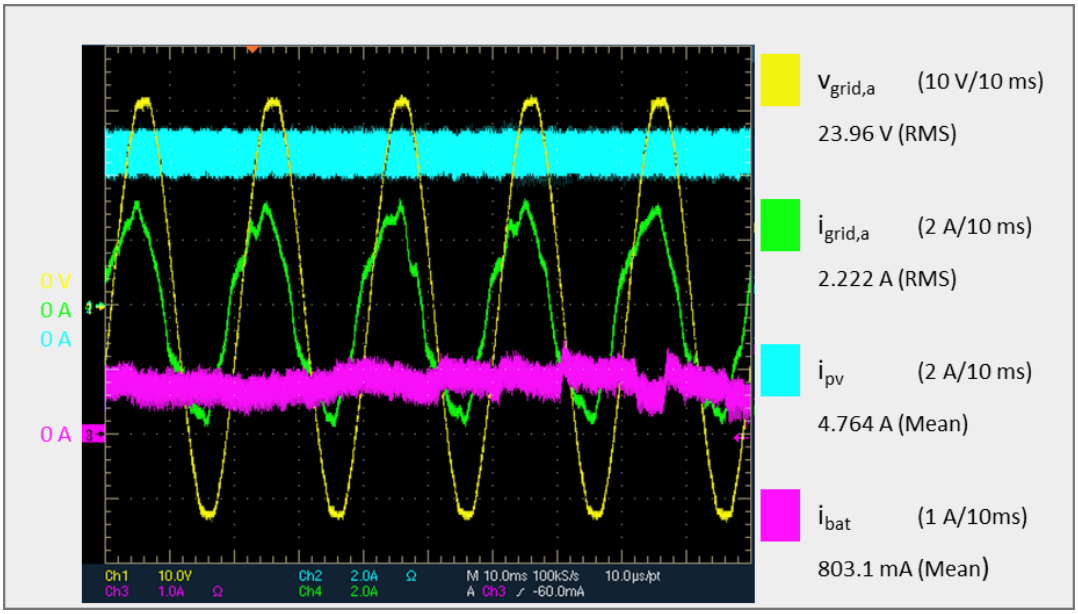

Figure 22. Scenario 3: Injected current to the grid in phase A ($i_{grid,a}$), grid voltage in phase A ($v_{grid,a}$), PV current (i_{pv}) and battery current (i_{bat}).

8.4 Scenario 4

Another ancillary service that the ER is able to perform when it is operating in an imbalanced grid, is the ability to inject different currents per phase in order to balance the demanded powers by single-phase loads. Figure 23 shows the injected currents in each phase A, B and C ($i_{grid,a}$, $i_{grid,b}$, $i_{grid,c}$ respectively). A good tracking of the coefficient unbalance per phase, given as independent references was demonstrated ($K_{unb,a}$, $K_{unb,b}$ and $K_{unb,c}$ are equal to 1.0, 0.4 and 0.8 respectively).

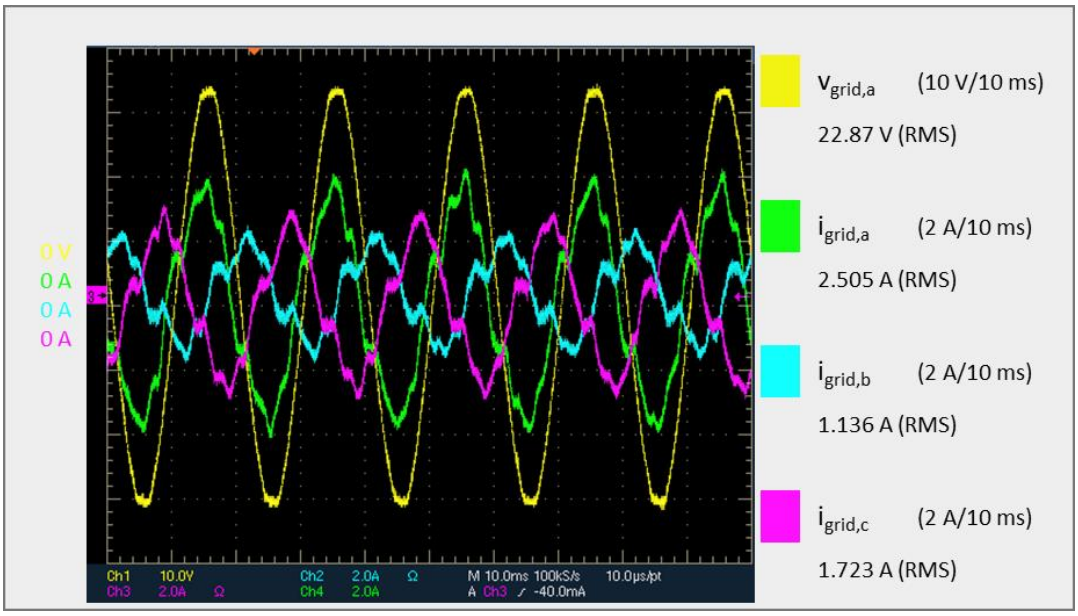

Figure 23. Scenario 4: Injected currents to grid in phases A, B and C ($i_{grid,a}$, $i_{grid,b}$, $i_{grid,c}$) and grid voltage in phase A ($v_{grid,a}$).

8.5 Scenario 5

This section analyses the main waveforms during transient responses under different reference steps. Figure 24 shows the initial situation when just pure active power obtained from the PV source and the ESS is injected to the grid. Figure 25 represents the injection of reactive power after receiving a new set-point. Figure 26 illustrate the situation of imbalance compensation by injecting different currents per phase.

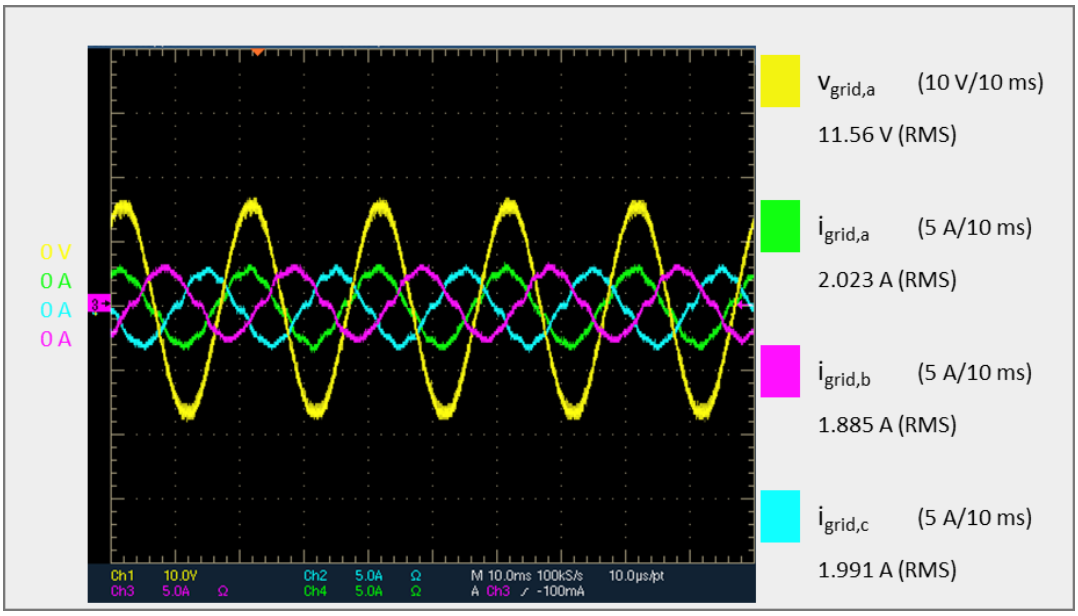

Figure 24. Scenario 5, active power injection: Injected currents to grid in phases A, B and C ($i_{grid,a}$, $i_{grid,b}$, $i_{grid,c}$) and grid voltage in phase A ($v_{grid,a}$).

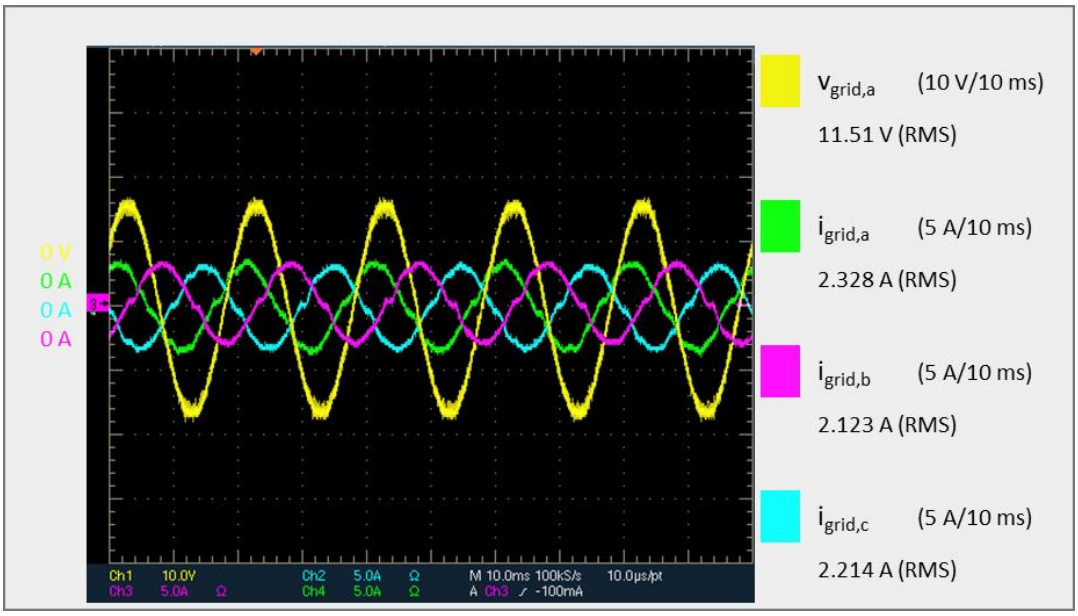

Figure 25. Scenario 5, active and reactive power injection: Injected currents to grid in phases A, B and C ($i_{grid,a}$, $i_{grid,b}$, $i_{grid,c}$) and grid voltage in phase A ($v_{grid,a}$).

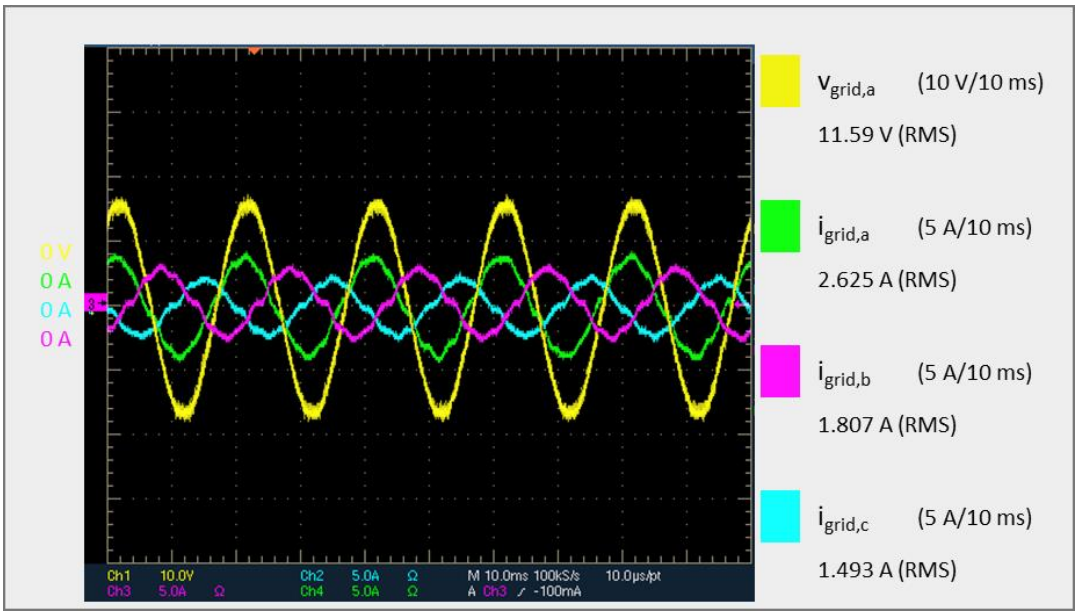

Figure 26. Scenario 5, imbalance compensation: Injected currents to grid in phases A, B and C ($i_{grid,a}$, $i_{grid,b}$, $i_{grid,c}$) and grid voltage in phase A ($v_{grid,a}$).

Figure 27 shows the evolution of the battery current when a positive to negative set-points are given in a step way (battery change from discharging to charging mode). The tracking of the reference value is accurate. It is important to note the any reference step is smoothed out by a ramp control.

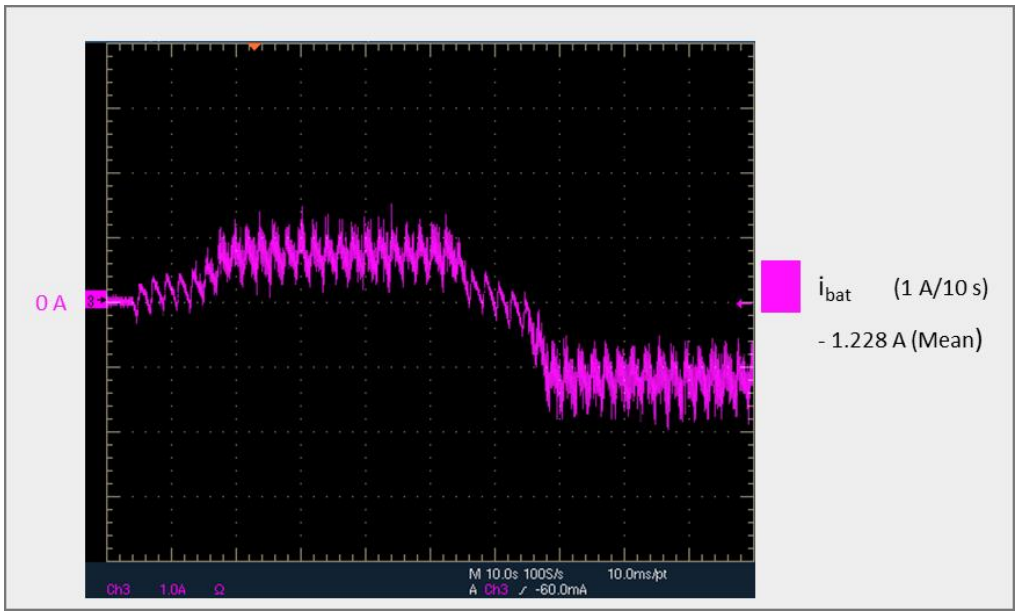

Figure 27. Scenario 5: Evolution of the battery current (i_{bat}) under a reference step change.

Figure 28 shows the long-term evolution of the active or reactive power in each system (PV array, ESS and utility grid) in different set-points. Figure 28 a) represents the continuous tracking of the maximum power point. The presented ripple is justified by the tracking method based on P&O. The exchanged power between the ESS and the common DC-link of the system is depicted in Figure 28 b). A charging/discharging cycle (its reference varies from 150 W to -150 W) is represented. The corresponding active power and the desired reactive power injected to the main grid are represented in Figure 28 c) and d) respectively. In the scenario of reactive power test, the ability to inject or demand reactive power (inductive or capacitive behaviour) was demonstrated.

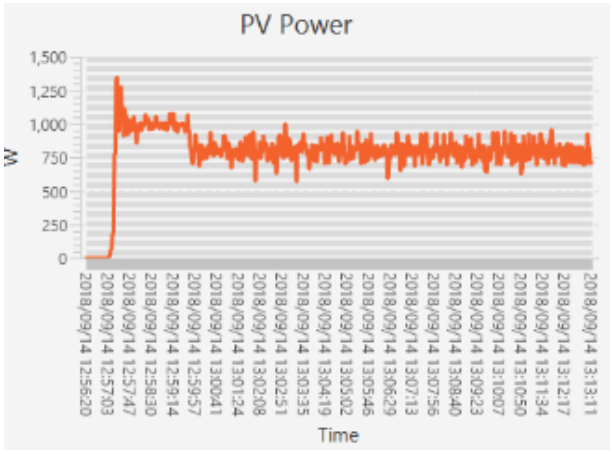

a)

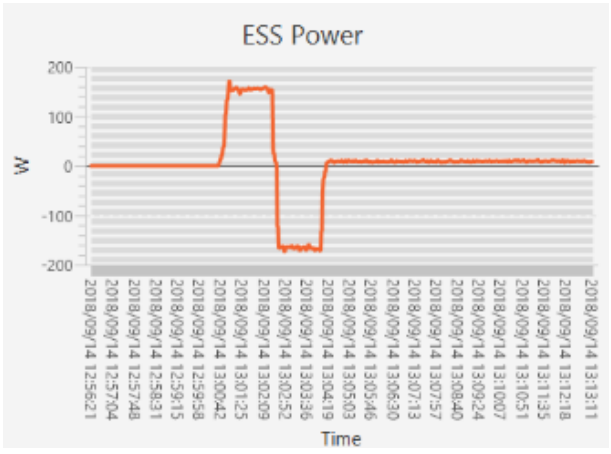

b)

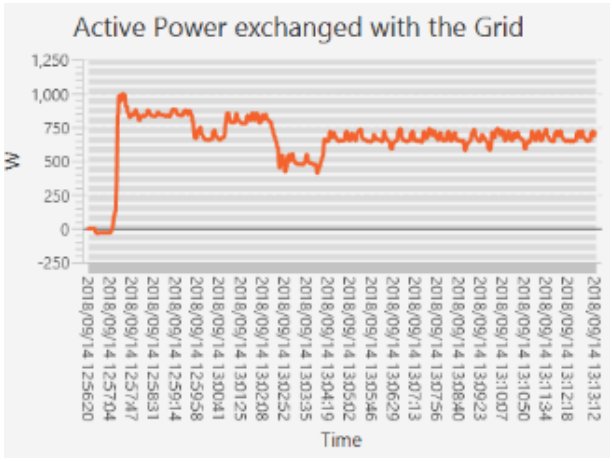

c)

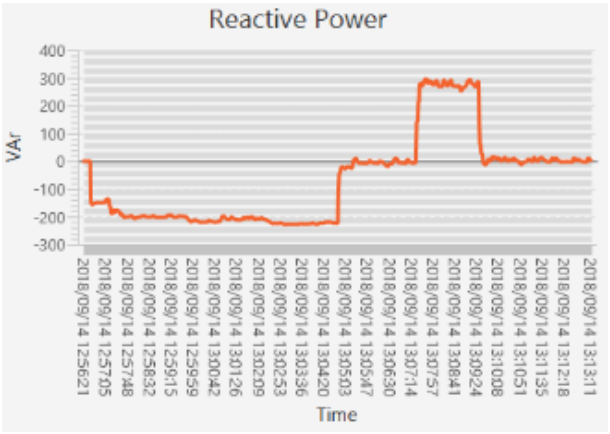

d)

Figure 28. Scenario 5: Different responses of the subsystems: a) PV power, b) Power exchanged with the ESS, c) Active power exchanged with the utility grid, and d) Reactive power.

9 On-site tests

The ER was deployed during the week of October 22nd to 26th 2018, and tested during the last two days. Unfortunately, due to the cloudy weather conditions (Figure 29), it was not possible to extract more than 100 W of the PV system during the on-site tests.

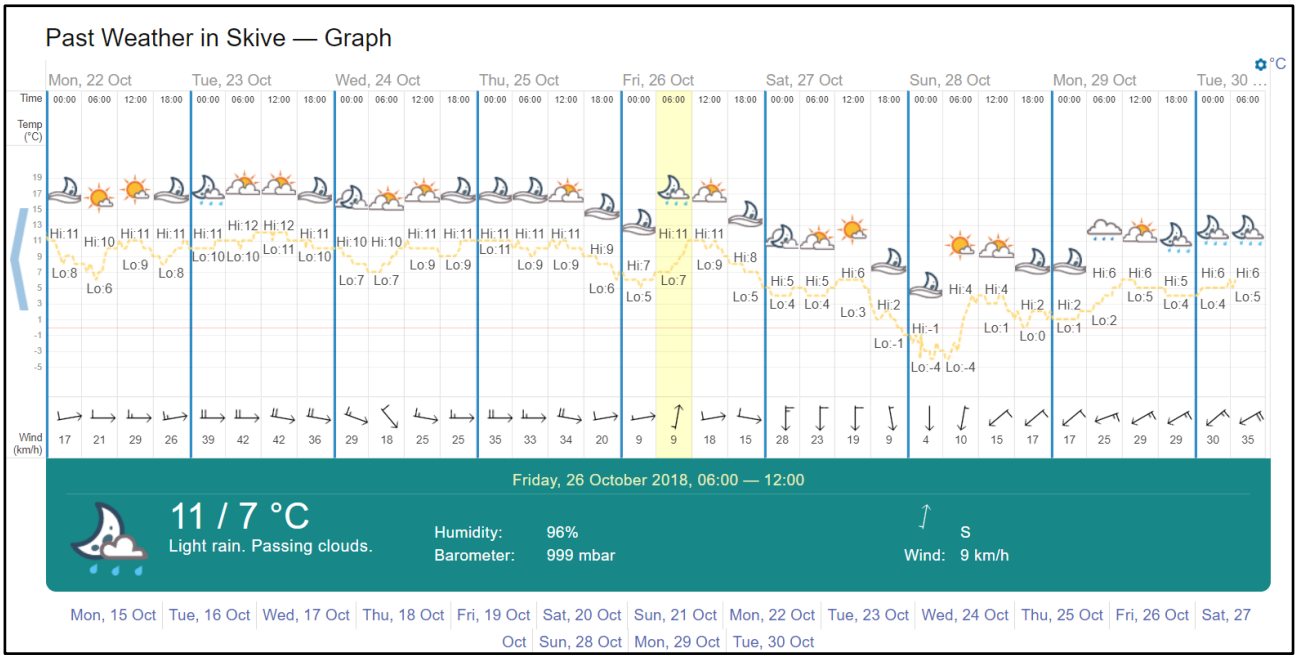

Figure 29. Weather conditions during the last on-site test day (October 26th, 2018)[v].

Despite that, the same five scenarios were tested at ENIIG's premises, namely:

1) PV system is operating at standard conditions, ESS discharges and DC-AC power converter is injecting pure active power into the main grid.
2) PV system is operating at standard conditions, ESS charges and DC-AC power converter is injecting the remaining pure active power into the main grid.
3) PV system is operating at standard conditions, ESS discharges and DC-AC power converter is injecting reactive power and active power into the main grid.
4) PV system is operating at standard conditions, ESS discharges and DC-AC power converter is injecting unbalanced currents into the main grid.
5) Transient analysis.

9.1 Scenario 1

The first on-site test aimed to validate the proper operation of the full system in terms of active power balance between the energy source, storage system and the utility grid. The main waveforms are represented in Figure 30. i_{pv} achieves the MPPT current according to the on-site current measured values (I_{sc} = 0.5 A). It was observed that the PV converter was working in Discontinuous Current Conduction Mode (DCCM) due to the low PV power available (around 100 W). The proper ESS operation was also validated with a $P_{bat,ref}$ equal to 100 W. Figure 31 shows the resulting power injected to the utility grid. Phase B of the current ($i_{grid,b}$) and phase B of the voltage ($v_{grid,b}$) present a similar shift. Due to the low irradiance, the injected power has a higher distortion.

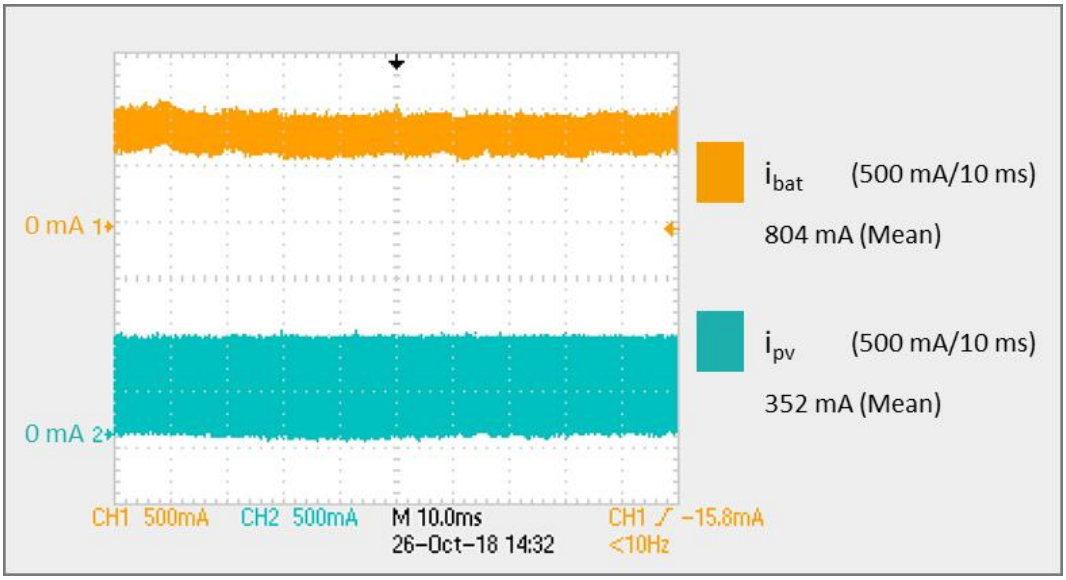

Figure 30. Scenario 1: PV current (i_{pv}) and battery current (i_{bat}).

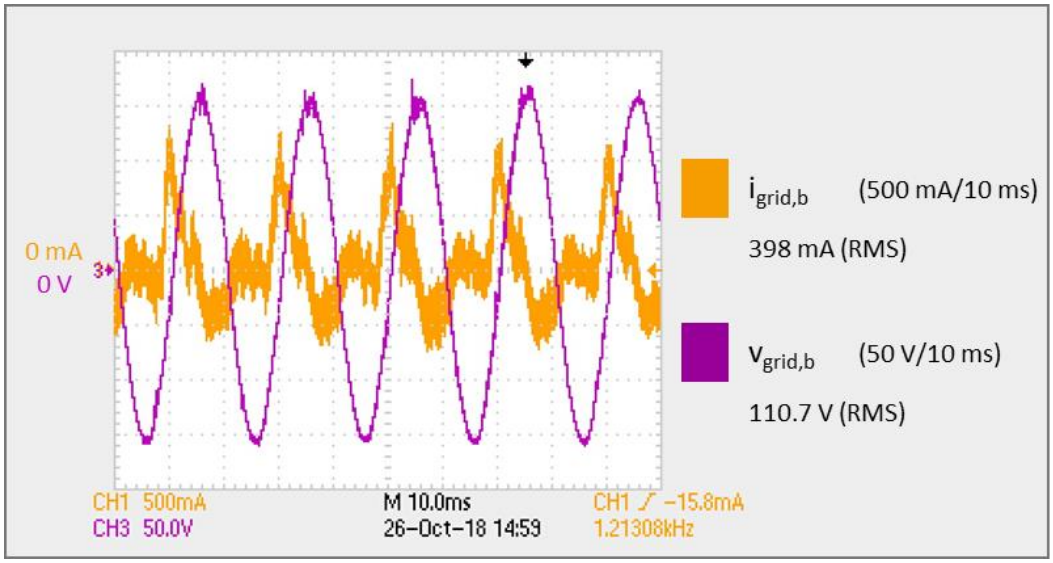

Figure 31. Scenario 1: Injected current to the grid in phase B ($i_{grid,b}$) and grid voltage in phase B ($v_{grid,b}$).

9.2 Scenario 2

Similar to scenario 1, the i_{pv} in Figure 32 shows a good tracking of the current at maximum power (i_{mpp}) despite the DC-DC boost converter works in DCCM. In this scenario, the ESS is being charged with a $P_{bat,\_ref}$ equals to -100 W, thus the battery current (i_{bat}) is negative.
Figure 33 shows the remaining power injected to the utility grid, the phase B of the current ($i_{grid,b}$) and the phase B of the voltage ($v_{grid,b}$).

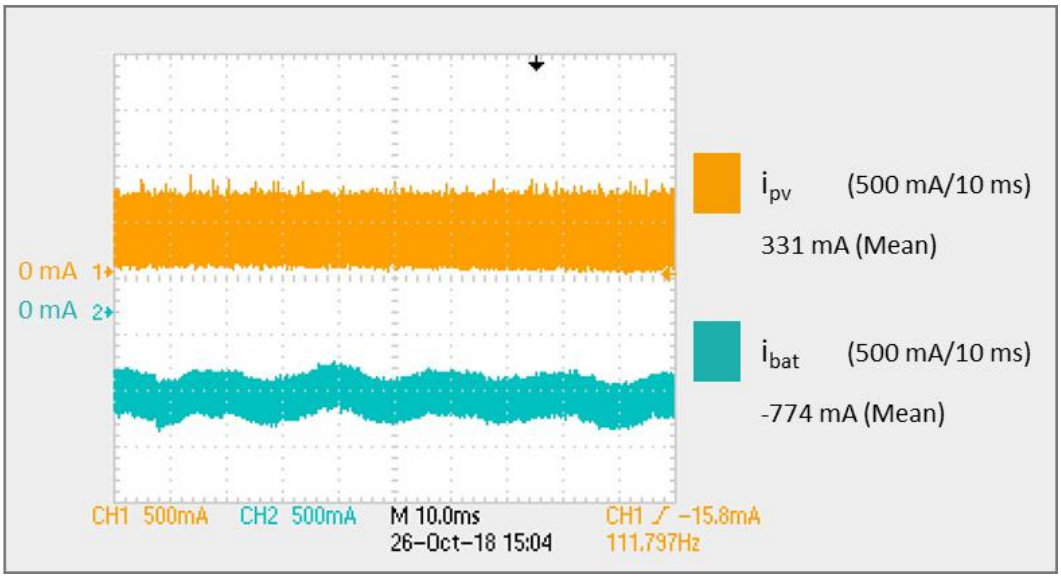

Figure 32. Scenario 2: PV current (i_{pv}) and battery current (i_{bat}).

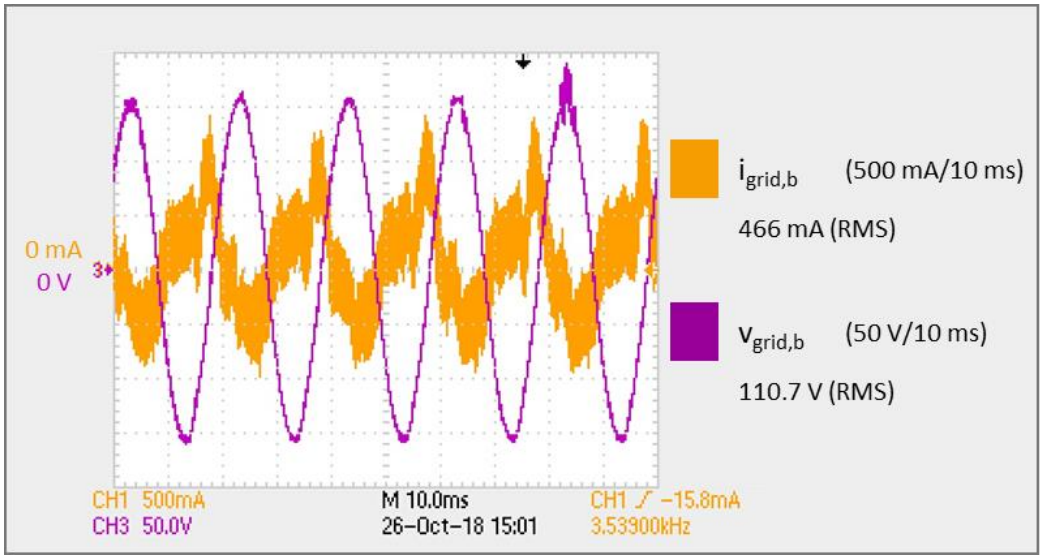

Figure 33. Scenario 2: Injected current to the grid in phase B ($i_{grid,b}$) and grid voltage in phase B ($v_{grid,b}$).

9.3 Scenario 3

In this scenario it was tested the ER capability to inject reactive power into the grid. Figure 34 shows the PV current (i_{pv}) which is extracting the maximum power from the PV source (around 100 W). The battery current (i_{bat}) has a discharging value corresponding to 100 W.
Figure 35 shows the resulting injected active and reactive power ($Q_{grid,ref}$ equals to 450 VAr) to the utility grid. It can be observed that the phase B grid current ($i_{grid,b}$) and phase B grid voltage ($v_{grid,b}$) are shifted.

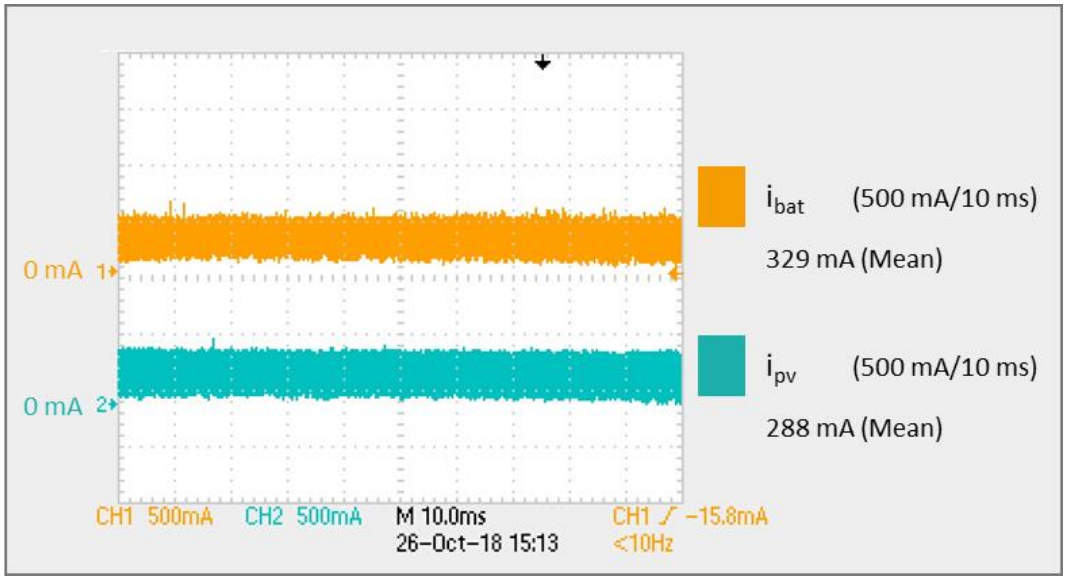

Figure 34. Scenario 3: PV current (i_{pv}) and battery current (i_{bat}).

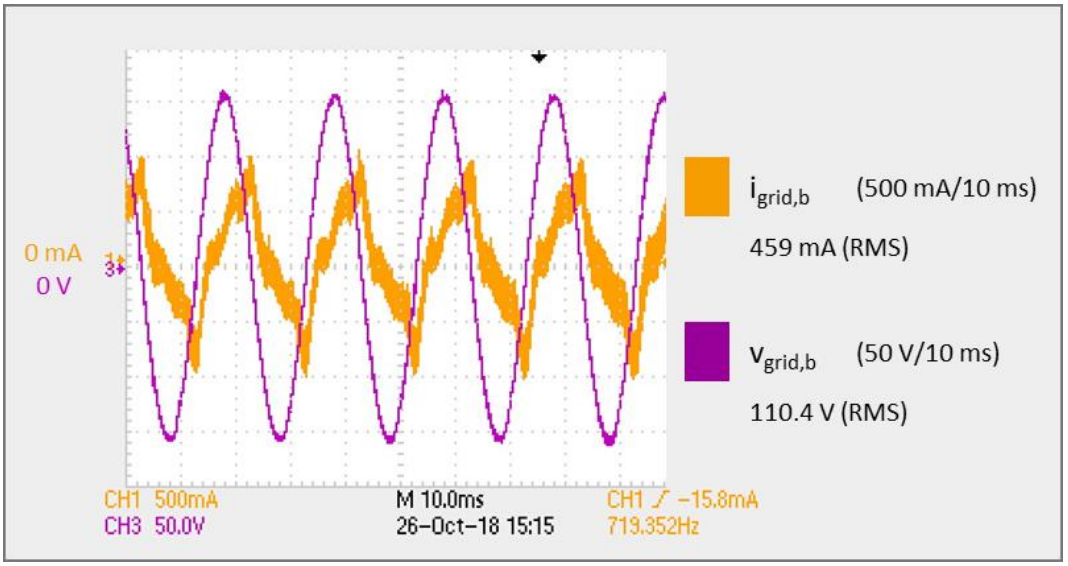

Figure 35. Scenario 3: Injected current to the grid in phase B ($i_{grid,b}$) and grid voltage in phase B ($v_{grid,b}$).

9.4 Scenario 4

This scenario demonstrates the ER ability to inject different currents per phase in order to balance the demanded powers by single-phase loads. Figure 36 shows the injected currents in phases B and C ($i_{grid,b}$, $i_{grid,c}$ respectively).

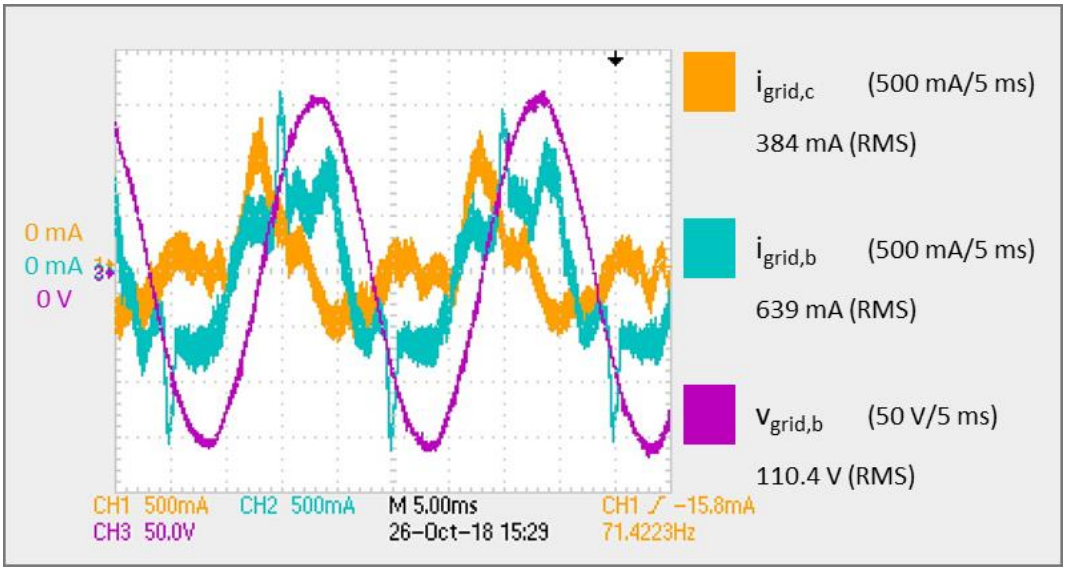

Figure 36. Scenario 4: Injected currents to grid in phases B and C ($i_{grid,b}$, i_{grid}) and grid voltage in phase B ($v_{grid,b}$).

9.5 Scenario 5

This section shows the system transient response under different reference steps. Figure 37 shows the evolution of the active or reactive power in each system (PV array, ESS and utility grid) in different set-points. Figure 37 a) represents the continuous tracking of the maximum power point. The presented ripple is justified by the tracking method based on P&O and the low irradiance during the on-site tests. The exchanged power between the ESS and the common DC-link of the system is depicted in Figure 37 b). A charging/discharging cycle (its reference varies from 100 W to -100 W) is represented. The corresponding active power and the desired reactive power injected to the main grid are represented in Figure 37 c) and d) respectively. In this scenario of reactive power test, the ability to inject or demand reactive power (inductive or capacitive behaviour) was demonstrated.

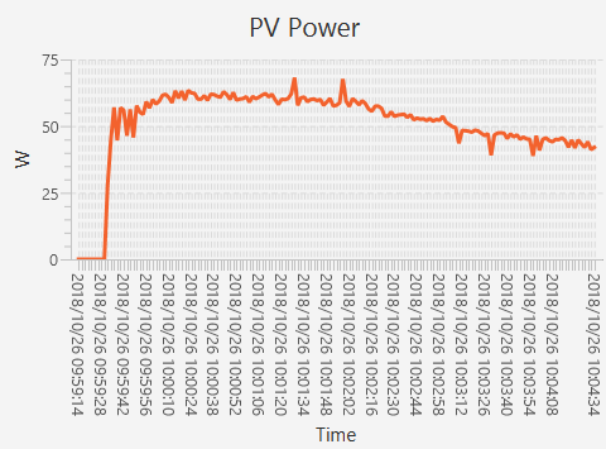

a)

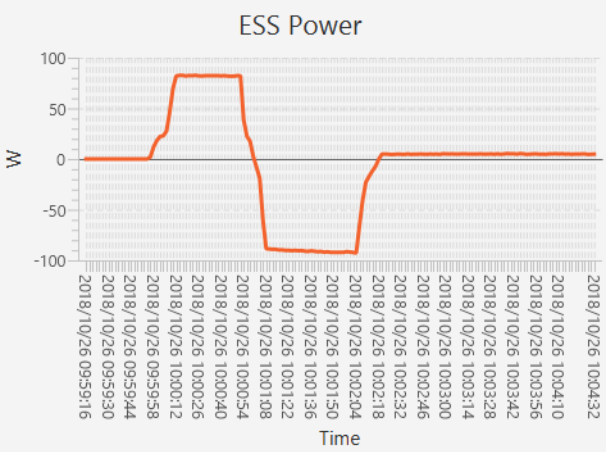

b)

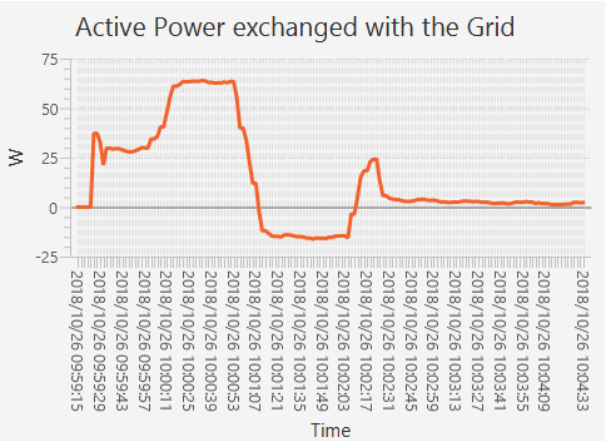

c)

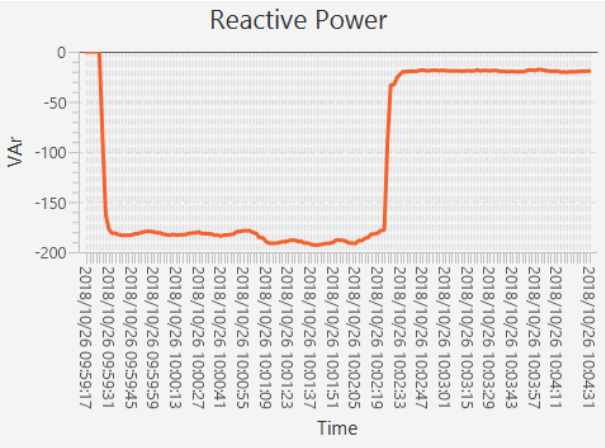

d)

Figure 37. Scenario 5: Different responses of the subsystems: a) PV power, b) Power exchanged with the ESS, c) Active power exchanged with the utility grid, and d) Reactive power.

10 Deployment problems

During deployment it was observed that the ER transformer had suffered a mechanical deformation during the transportation to the test site. However, it did not affect the deployment and the on-site tests. Chapter 0 showed the correct ER operation. Nevertheless, there is a very small possibility that the transformer creates a hot spot and causes a fire in the room due to this deformation. Because of this and the presence of a large number of batteries inside the room the danger is big. Since the security of the persons in the building is the top priority, the ER was left disconnected from the grid. Its correct operation can be verified at any time, with human supervision in the ER room.

Figure 38 shows the transformer magnetization currents in phase A and B. Theses currents should have similar waveform and amplitude, but since the ER transformer is damaged, it is possible to observe that phase B current has a value of 413 mA, while the current in the damaged phase A has a value of 648 mA. The ER transformer is planned to be changed with a new one in the very near future.

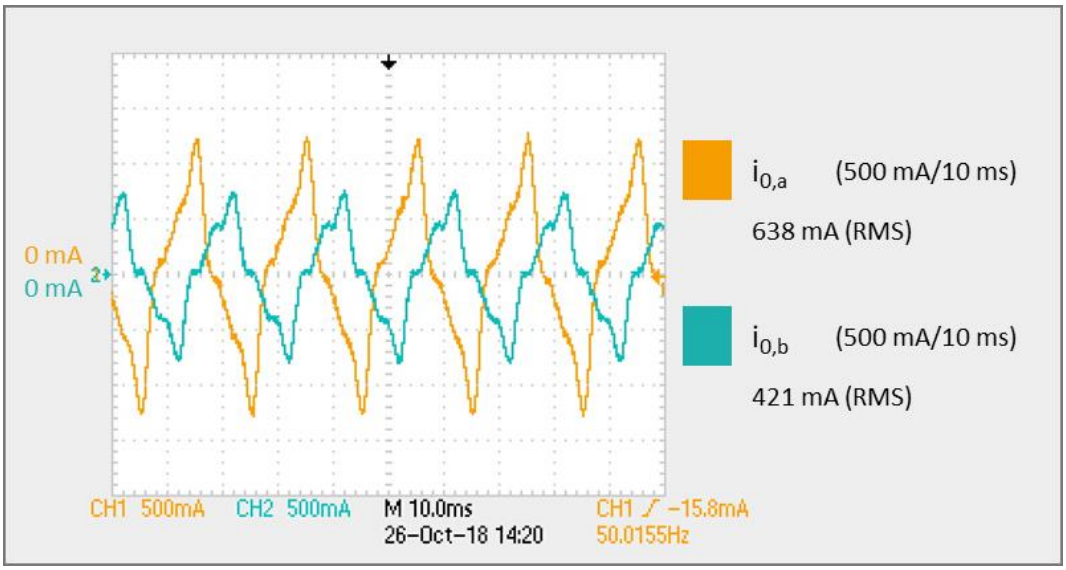

Figure 38. Transformer magnetization currents in phase A ($i_{0,a}$) and B ($i_{0,b}$).

11 Installation/Deployment instructions

An ER SMX SB connector needs to be present in the SMX to enable the interaction with the three-phase ER. This component is detailed described in D4.9 [S4G-D4.9].

The ER deployment instructions are very extensive and require a very specific expertise. For this reason, the ER deployment should only be performed by the UNINOVA partner. Figure 39 shows the front view of the ER cabinet with the different components, while Figure 40 shows the rear view. Figure 41 shows the ER deployed at ENIIG's premises. Figure 42 shows the ER GUI which enables the local control and monitoring of the ER operation.

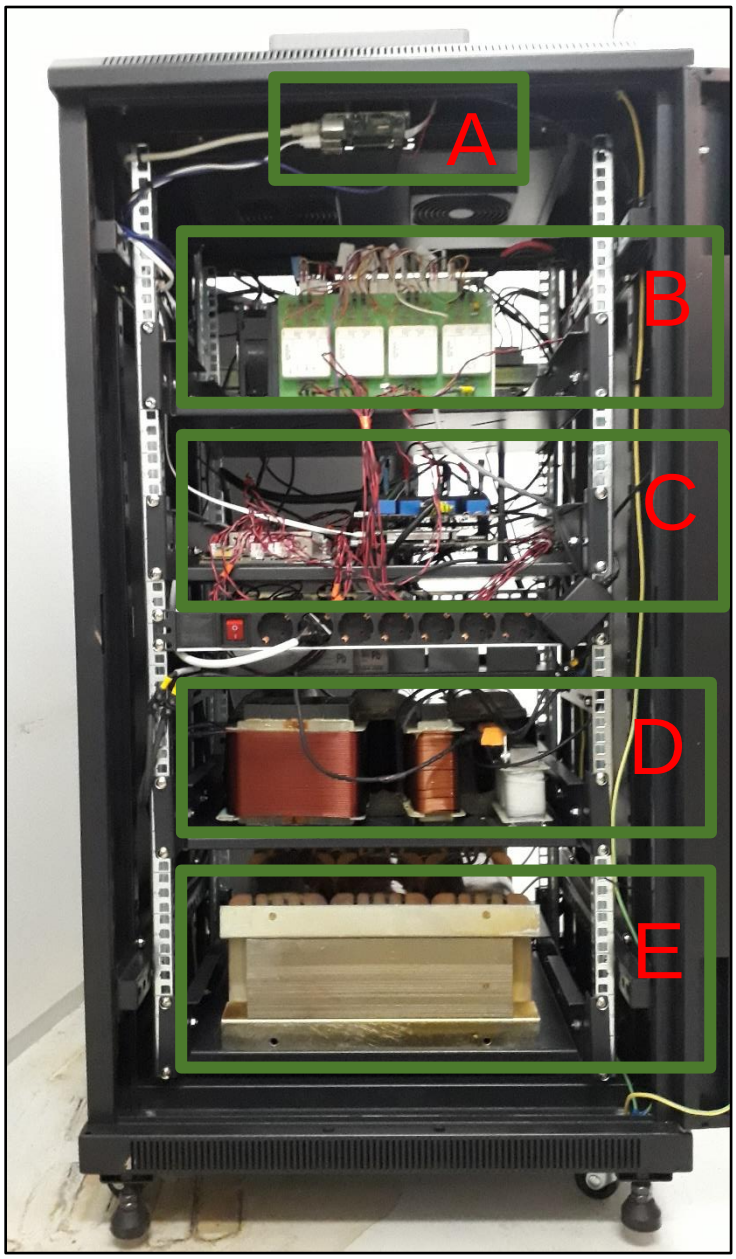

Figure 39. ER cabinet front view (A – ER controller; B – PV, ESS and grid power converters; C – measurement and control boards; D – inductance filters; E – transformer).

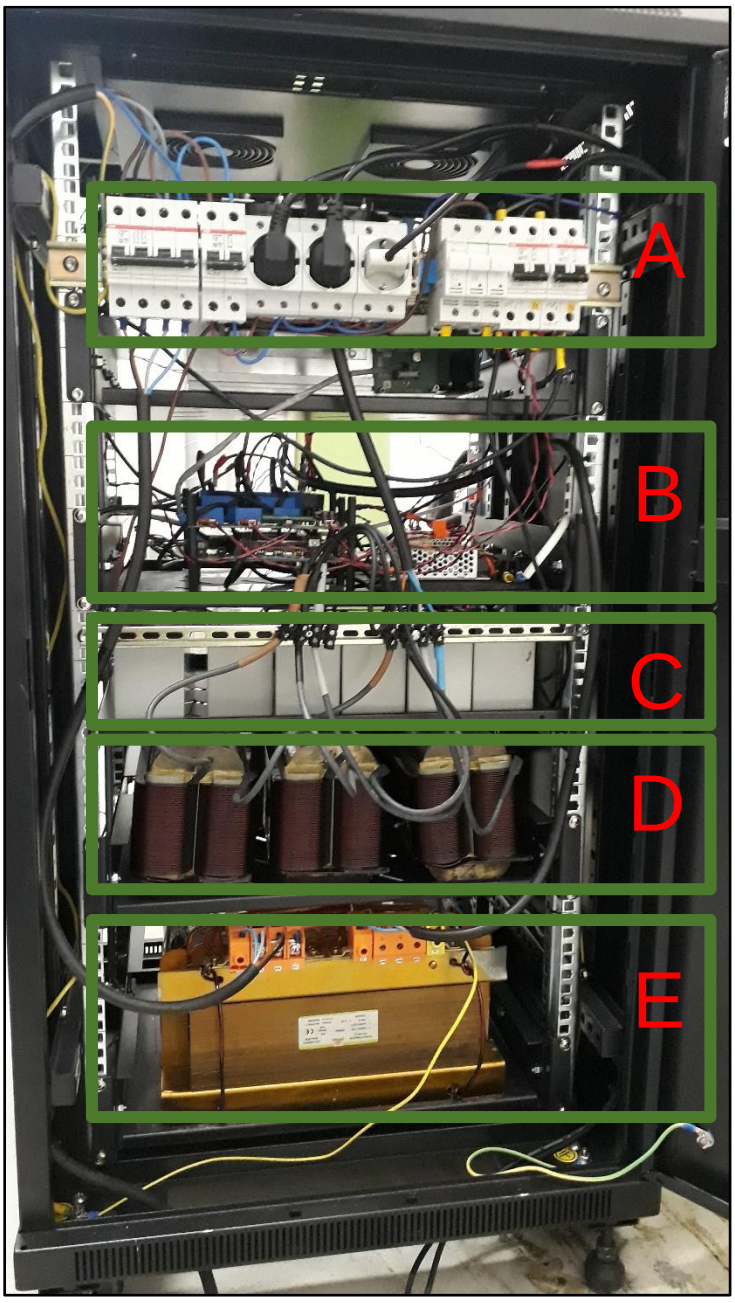

Figure 40. ER cabinet rear view (A – circuit breakers; B – measurement and control boards; C – ESS; D – inductance filters; E – transformer).

Figure 41. ER deployed at ENIIG's premises.

Figure 42. ER GUI for local control and monitoring.

12 Conclusions

A comprehensive simulation study was performed in the PSCAD/EMTDC[i] software to validate the sizing values, the main functionalities, control algorithms, and modulation methods for the three-phase ER prototype. Different scenarios were defined in order to validate the correct operation of the three-phase ER, namely:

1) PV system is operating at standard conditions, ESS discharges and DC-AC power converter is injecting pure active power into the main grid.
2) PV system is operating at standard conditions, ESS charges and DC-AC power converter is injecting the remaining pure active power into the main grid.
3) PV system is operating at standard conditions, ESS discharges and DC-AC power converter is injecting reactive power and active power into the main grid.
4) PV system is operating at standard conditions, ESS discharges and DC-AC power converter is injecting unbalanced currents into the main grid.
5) Transient analysis.

The scenarios were analysed and simulated, showing a correct operation of the ER in all the different scenarios. The three-phase ER prototype was tested in laboratory and validated at the ENIIG's premises, obtaining similar results. Despite the ER transformer issue, the correct ER operation can be verified at any moment with human supervision in the ER room. The ER transformer is planned to be changed with a new one in the very near future.

Acronyms

Acronym	Explanation
AC	Alternating Current
C	Capacitor
D	Diode
DC	Direct Current
DCCM	Discontinuous Current Conduction Mode
ER	Energy Router
ESR	Equivalent Series Resistor
ESS	Energy Storage System
GUI	Graphical User Interface
IGBT	Insulated-Gate Bipolar Transistors
L	Inductance
MPP	Maximum Power Point
MPPT	Maximum Power Point Tracking
P	Active power
P&O	Perturb and Observe
PV	Photovoltaic
PWM	Pulse Width Modulation
Q	Reactive power
RMS	Root Mean Square
RPPT	Reference Power Point Tracking
S	Switch
SMX	Smart Meter eXtension
SoC	State of Charge

Variables nomenclature

Variables	Description
η	Efficiency
Δ_{IL}	Inductor ripple current
Δ_{Vdc_link}	Output DC-link voltage ripple
f_s	Minimum switching frequency
ω_1	Fundamental harmonic
$C_{dc\_link,m}$	Minimum DC-link capacitor
D_{bat}	Maximum battery duty cycle
D_{pv}	Maximum PV duty cycle
h_{SW}	Switching harmonic number
i_{bat}	Battery current
$I_{d,ref}$	Direct component reference current
$i_{grid,a}$	Phase A grid current
$i_{grid,b}$	Phase B grid current
$i_{grid,c}$	Phase C grid current
$i_{pv,M}$	Maximum PV output current
$i_{bat,M}$	Maximum battery pack output current
I_{mpp}	Maximum power point current
i_{pv}	PV current
I_{sc}	Short-circuit current
I_{SW}	Grid RMS harmonic current at the switching frequency
$K_{unb,a}$	Phase A unbalance coefficient
$K_{unb,b}$	Phase B unbalance coefficient
$K_{unb,c}$	Phase C unbalance coefficient
P_{bat}	Nominal battery pack power
$P_{bat,ref}$	Battery power reference
$Q_{grid,ref}$	Reactive power grid reference
V_{bat}	Nominal battery pack voltage
$v_{grid,a}$	Phase A grid voltage
$V_{i(hSW)}$	Converter output voltage at the switching frequency
V_{mpp}	Maximum power point voltage

$V_{bat,m}$	Minimum battery input voltage
$V_{bat,M}$	Maximum battery input voltage
$V_{pv,m}$	Minimum PV input voltage
$V_{pv,M}$	Maximum PV input voltage
V_{oc}	Open circuit voltage
V_{dc_link}	Nominal output voltage

List of figures

List of tables

References

[i] PSCAD, *Power systems computer-aided design*, https://hvdc.ca/, accessed 08 October 2018.
[ii] CEI 0-21, *Reference technical rules for the connection of active and passive users to the LV electrical Utilities*, https://www.mcenergy.it/images/CEI-0-21.pdf, accessed 08 October 2018
[iii] FGW TR3, *Technical Guidelines*, https://wind-fgw.de/themes/working-on-the-guidelines/?lang=en, accessed 08 October 2018
[iv] Decree Law 1565/2010, *Real Decreto 1565/2010, de 19 de noviembre, por el que se regulan y modifican determinados aspectos relativos a la actividad de producción de energía eléctrica en régimen especial*, https://www.boe.es/boe/dias/2010/11/23/pdfs/BOE-A-2010-17976.pdf, accessed 08 October 2018 [Spanish]
[v] TimeAndDate, *Past weather in Skive - Denmark*, https://www.timeanddate.com/weather/denmark/skive/historic, accessed 30 October 2017.